REPORT DOCUMENTATION PAGE

Form Approved
OMB No. 0704-0188

PLEASE DO NOT RETURN YOUR FORM TO THE ABOVE ORGANIZATION.

1. REPORT DATE *(DD-MM-YYYY)*	2. REPORT TYPE	3. DATES COVERED *(From - To)*
28-2-2012	Final Technical	1-3-2009 - 30-11-2011

4. TITLE AND SUBTITLE
Measurements of the Mechanisms of Laminar-Turbulent Transition in the Mach-6 Quiet Tunnel

5a. CONTRACT NUMBER

5b. GRANT NUMBER
FA9550-09-1-0191

5c. PROGRAM ELEMENT NUMBER

6. AUTHOR(S)
Steven P. Schneider

5d. PROJECT NUMBER

5e. TASK NUMBER

5f. WORK UNIT NUMBER

7. PERFORMING ORGANIZATION NAME(S) AND ADDRESS(ES)
Purdue University, School of Aeronautics and Astronautics
1375 Aviation Drive
West Lafayette, IN 47907-2015

8. PERFORMING ORGANIZATION REPORT NUMBER

9. SPONSORING/MONITORING AGENCY NAME(S) AND ADDRESS(ES)
Air Force Office of Scientific Research
875 N. Randolph St
Suite 325, Room 3112
Arlington, VA 22203

10. SPONSOR/MONITOR'S ACRONYM(S)
AFOSR

11. SPONSOR/MONITOR'S REPORT NUMBER(S)
AFRL-OSR-VA-TR-2012-0386

12. DISTRIBUTION/AVAILABILITY STATEMENT
Approved for public release, distribution unlimited

13. SUPPLEMENTARY NOTES

14. ABSTRACT
The Mach-6 tunnel continues to run quiet to moderately high Reynolds numbers. Quiet flow was degraded in 2010 when the throat was opened, but a thorough repolishing of the throat resulted in a significant improvement in performance. Since the nozzle-wall boundary layer remains laminar more than 10 inches downstream of the exit to unit Reynolds numbers near 3.5 million per foot, unprecedented quiet-flow Reynolds numbers can now be achieved on slender models. The tunnel is operated by a single graduate student, with good reliability, and a large amount of data can be obtained during each run using a variety of sensors. Instability and transition measurements were carried out on various models to study the second-mode and crossflow instabilities, the instabilities behind an isolated roughness, the development of second-mode wave packets and turbulent spots, the general effects of roughness and tunnel noise, the effect of tunnel noise on oscillations in a forward-facing cavity, and other phenomena. The research resulted in 17 conference papers, 8 Master's theses and 2 Ph.D. theses. A brief summary is reported here, along with selected highlights

15. SUBJECT TERMS
hypersonic laminar turbulent transition experiments quiet wind tunnels

16. SECURITY CLASSIFICATION OF:			17. LIMITATION OF ABSTRACT	18. NUMBER OF PAGES	19a. NAME OF RESPONSIBLE PERSON
a. REPORT	b. ABSTRACT	c. THIS PAGE			Steven P. Schneider
U	U	U	unlimited	37	19b. TELEPHONE NUMBER *(Include area code)* 765-494-3343

Reset

Final Report for AFOSR Grant FA9550-09-1-0191

1 Mar. 2009 to 30 Nov. 2011

Measurements of the Mechanisms of Laminar-Turbulent Transition in the Mach-6 Quiet Tunnel

Steven P. Schneider, Professor
School of Aeronautics and Astronautics
Purdue University
Aerospace Sciences Lab
1375 Aviation Drive West Lafayette, IN 47907-2015

February 28, 2012

Summary

The Mach-6 tunnel continues to run quiet to moderately high Reynolds numbers. Quiet flow was degraded in 2010 when the throat was opened, but a thorough repolishing of the throat resulted in a significant improvement in performance. Since the nozzle-wall boundary layer remains laminar more than 10 inches downstream of the exit to unit Reynolds numbers near 3.5 million per foot, unprecedented quiet-flow Reynolds numbers can now be achieved on slender models. The tunnel is operated by a single graduate student, with good reliability, and a large amount of data can be obtained during each run using a variety of sensors. Instability and transition measurements were carried out on various models to study the second-mode and crossflow instabilities, the instabilities behind an isolated roughness, the development of second-mode wave packets and turbulent spots, the general effects of roughness and tunnel noise, the effect of tunnel noise on oscillations in a forward-facing cavity, and other phenomena. The research resulted in 17 conference papers, 8 Master's theses and 2 Ph.D. theses. A brief summary is reported here, along with selected highlights.

Contents

1 Introduction

The research performed under this grant is documented in a series of AIAA Papers [1, 2, 3, 4, 5, 6, 7, 8, 9, 10, 11, 12, 13, 14, 15, 16, 17]. As described in more detail below, some of the research was jointly funded by NASA or Sandia National Lab, and several students were supported in part by various fellowships. AFOSR funding is the foundation on which these collaborative efforts are built, and often provides critical elements in multi-organization joint efforts. Another review paper was revised into journal form, to help educate a new generation of engineers not familiar with the vast Cold War literature [18]. One of the conference papers appeared in journal form [19]. A number of students also completed theses [20, 21, 22, 23, 24, 25, 26, 27, 28, 29]. Since considerable detail is readily available in these publications, the present final report was written as an overall summary.

2 The Boeing/AFOSR Mach-6 Quiet Tunnel

2.1 General Description

Quiet facilities require low levels of noise in the inviscid flow entering the nozzle through the throat, and laminar boundary layers on the nozzle walls. To reach these low noise levels, conventional blow-down facilities must be extensively modified. Requirements include a 1 micron particle filter, a highly polished nozzle with bleed slots for the contraction-wall boundary layer, and a large settling chamber with screens and sintered-mesh plates for noise reduction [30]. To reach these low noise levels in an affordable way, the Purdue facility has been designed as a Ludwieg tube [31]. A Ludwieg tube is a long pipe with a converging-diverging nozzle on the end, from which flow exits into the nozzle, test section, and second throat, as shown in Fig. 1. A diaphragm is placed downstream of the test section. When the diaphragm bursts, an expansion wave travels upstream through the test section into the driver tube. Since the flow remains quiet after the wave reflects from the contraction, sufficient vacuum can extend the useful runtime to many cycles of expansion-wave reflection, during which the pressure drops quasi-statically.

The contraction-wall boundary layer is bled off just upstream of the throat, beginning a fresh undisturbed boundary layer for the nozzle wall. A fast valve is connected directly between the bleeds and the vacuum tank, allowing the bleed air to be dumped directly into the tank. If the bleed valves remain closed, the air entering the throat is disturbed by passing over the bleed slots, tripping the nozzle-wall boundary layer. Thus, these tunnels can run quiet and noisy at nearly the same operating condition, by opening or closing the bleed valves.

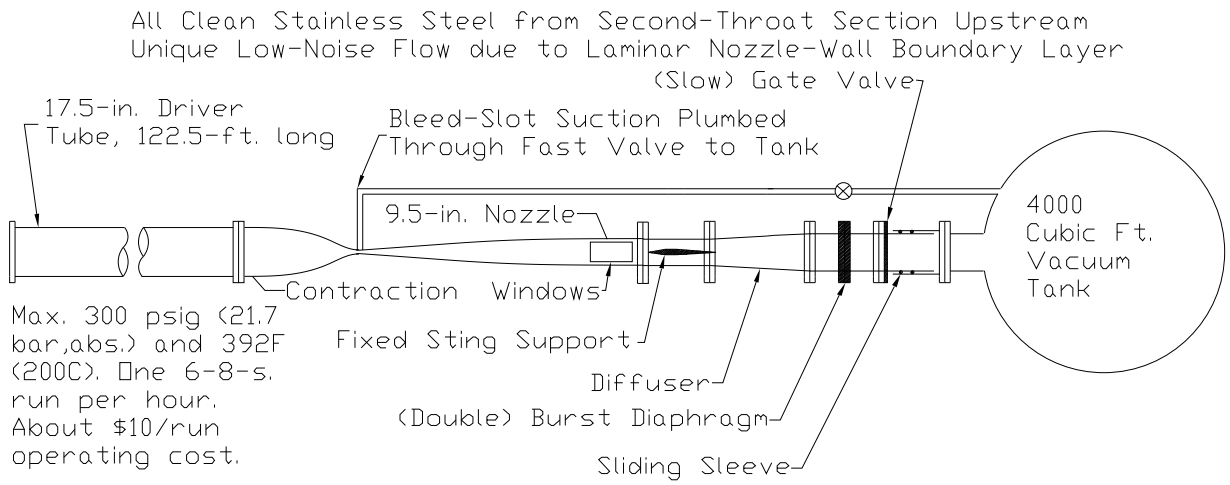

Figure 1: Schematic of Boeing/AFOSR Mach-6 Quiet Tunnel

Unless otherwise specified, the initial stagnation temperature in the driver tube is set to $160°C$. The stagnation temperature drops about 10% during the run, as the air flows out of the driver tube [32]. The air in the nozzle at Mach 6 is supercooled, making Reynolds number computations dependent on the somewhat uncertain value of air viscosity at very low temperatures, but no evidence of condensation has been observed under these conditions [33], although further studies are needed.

Figure 2 shows the nozzle. Here, z is an axial coordinate whose origin is at the nozzle throat. The region of useful quiet flow lies between the characteristics marking the onset of uniform flow, and the characteristics marking the upstream boundary of acoustic radiation from the onset of turbulence in the nozzle-wall boundary layer. A 7.5-deg. sharp cone is drawn on the figure. The rectangles are drawn on the nozzle at the location of window openings, all but one of which are presently filled with blank metal inserts. Images of the tunnel are available at `http://roger.ecn.purdue.edu/~ aae519/BAM6QT-Mach-6-tunnel/`, along with earlier papers and other documentation.

2.2 Status and Improvements for FY09-11

The tunnel operated fairly reliably for the duration of the grant, but did suffer from intermittent downtime. The quiet-flow performance is exquisitely sensitive to the cleanliness and polish in the nozzle throat, so it varies from time to time. The tunnel is operated by a single researcher, usually a graduate student, and available labor has been sufficient to keep the tunnel operating about 45-50 weeks per year, for roughly 25 shots per week on average. Although it now takes a minimum of about 35 minutes between successive runs under ideal conditions, a substantial portion of a student's occupancy time is usually expended in model setup and adjustment, debugging apparatus, and so on. Thus, about 9 runs is the maximum that is usually feasible in a 10-hour day.

Since downtime interrupts research progress, and is particularly difficult when outside researchers travel to Purdue to use the tunnel, several projects were undertaken to improve performance and reliability. A second 25HP vacuum pump was procured and wired in 2008

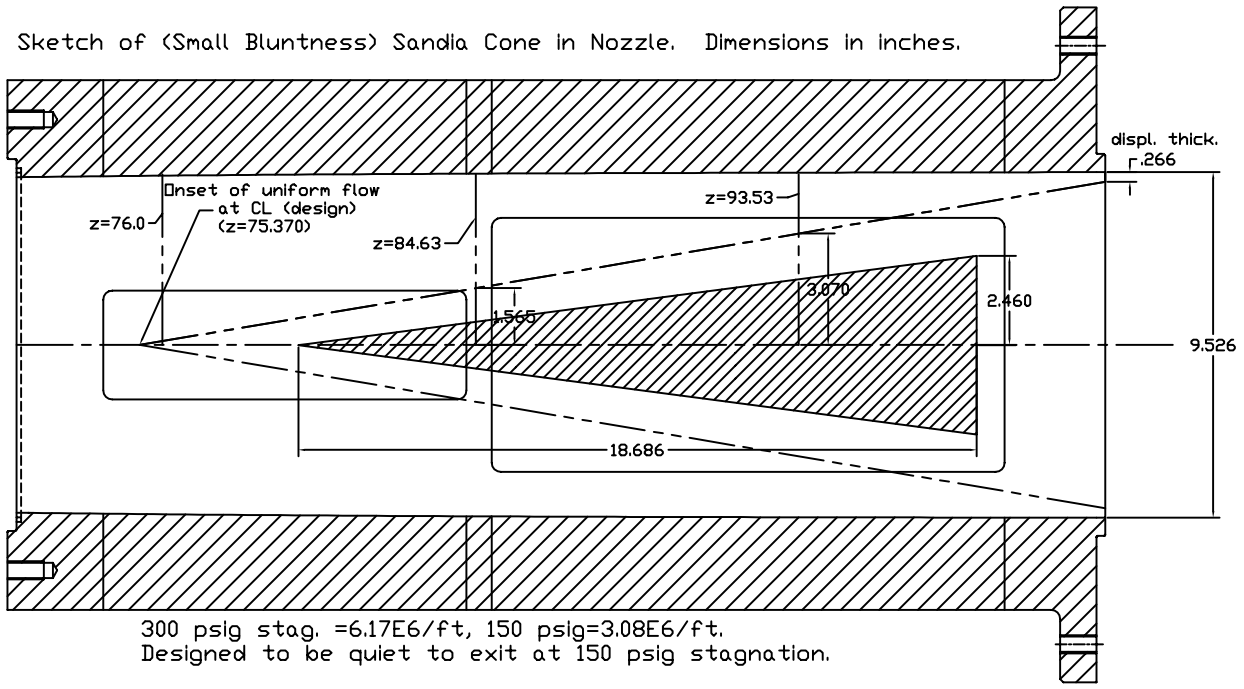

Figure 2: Schematic of Mach-6 Quiet Nozzle with Model

to reduce the time between runs. The two pumps are nearly identical, to reduce maintenance costs. One pump can lower the pressure in the 4000 cf tank to a few torr in about an hour, while two pumps reduce this to about a half-hour. Low downstream pressures are necessary for achieving hypersonic flow at moderate Reynolds numbers, leading to the requirement for a vacuum system. Vacuum pumps and a vacuum tank are an order of magnitude more efficient than high-pressure injectors, although feasible tank sizes tend to limit runtime to a few seconds. During 2009, the control systems were debugged and the second pump was put into routine operation. This has provided a substantial improvement in research productivity, so the researcher is no longer waiting for the vacuum pump when preparing for the next run. The second pump also provides redundancy, so tunnel operations can continue even when one of the two pumps is out of service.

A FY2008 DURIP grant was to improve performance and reliability by procuring a new throat, machined from stainless steel [34]. However, difficulties with the vendor and the throat fabrication left this project incomplete, regrettably. Funding to complete this throat needs to be located, or the tunnel will eventually lose quiet flow, due to unrepairable surface-finish flaws that can be expected to develop in the existing nozzle throat in the course of time. In an additional setback, the throat was opened several times in order to obtain precise measurements of the geometry of the mating parts, and this introduced dust into the nozzle, which apparently introduced some microscopic scratches [25]. In spring and summer 2010 this led to dramatic reductions in the quiet-flow performance [10]. However, the nozzle was repolished in August 2010, and after several months of operations quiet flow was achieved at the highest stagnation pressure yet observed, about 165 psia [12].

The tunnel has been operating for ten years, since 2001, and some of the parts are

beginning to wear out. A 12-inch gate valve was used to maintain vacuum in the 4000 cubic-foot tank while the burst diaphragms are being changed, in order to reduce the time between runs. The seal in this gate valve was failing, because the seating surfaces were accumulating damage from diaphragm impacts. Following a suggestion from AFRL/RB personnel, a 12-inch ball valve was procured and installed to replace it [15]. This valve seals much better, so it is also improving productivity. In addition, and surprisingly, this valve may also permit tunnel operation without burst diaphragms.

The 50HP first-stage compressor that provides 140 psig air for the facility has also suffered from intermittent reliability problems. The FY12-16 AFOSR grant proposal calls for replacing it with a slightly larger variable-speed compressor of much higher quality. Since this requires an upgrade to the electrical power connections, a 200A 480V 3-phase line was wired in 2011.

3 Instability and Transition on the X-51A

The beginning of the present grant saw the completion of Matt Borg's studies of transition on the X-51A [20]. These results were summarized in the final report for the previous grant. Transition on the lee side of the X-51A appears to involve the second-mode instability and also the crossflow instability, although the presence of the latter has not yet been confirmed. Tunnel noise has a marked effect on roughness-induced transition for both windward and leeward sides.

4 Instability and Transition on the HiFire-5

The beginning of the present grant also saw the completion of Tom Juliano's studies of the HiFire-5 [21, 9]. Transition on the centerline again appeared to result from the growth of second-mode waves, while off-centerline transition was apparently induced by the crossflow instability. These studies were continued by Matt Borg, who is now a contractor employed by AFRL/RB [35]. Although Borg et al. were funded directly by AFRL, several weeks in the Mach-6 quiet tunnel was supported by the present grant, and Juliano's HiFire-5 model was also provided. Borg et al. found traveling and possibly stationary crossflow waves, but only under quiet flow. Under noisy flow, the windward transition mechanism could not be determined. The effect of roughness on the attachment line was also determined, in order to help with the specifications for the flight vehicle. Once again, roughness-induced transition was delayed under quiet flow.

5 Second-Mode Wave Measurements on Sharp Cones in Several Wind Tunnels

5.1 Summary

Second-mode instability waves are being measured in several wind tunnels using PCB-132 sensors [36]. A sharp cone with a 7-deg. half-angle is being used in most of these experiments,

which are being carried out in numerous wind tunnels in the U.S. and overseas, by a variety of researchers, supported by various agencies. Although the work began in Japan, continued via a collaboration between T.U. Braunschweig and Purdue [37], and then continued with partial support from a separate AFOSR grant [36], funding from the present grant also helped to continue this cooperative effort. The research is generally aimed at determining the instability mechanisms responsible for Pate's correlation of transition on sharp cones at zero angle of attack in various wind tunnels [8]. If the noise levels and instability waves can be characterized in various tunnels, then the factors affecting second-mode transition could be determined. This information could then be used to predict second-mode transition on other geometries in these same wind tunnels, and perhaps also in flight [24]. Dennis Berridge is continuing the Purdue portion of this multinational effort for his Ph.D. thesis, funded in part by the present grant. Since Fall 2010, Berridge has also been supported as a NASA Langley graduate cooperative-education student, and since Fall 2011 he has also been supported by a NASA Aeronautics Scholarship. However, Berridge's experimental hardware continues to be funded by AFOSR.

5.2 Research Highlight: Growth of Second-Mode Waves with Unit Reynolds Number

A 7-deg. half-angle sharp-cone was studied at zero angle of attack in several wind tunnels [8]. Plots of spectra at different unit Reynolds numbers in three different tunnels show wave growth and breakdown (Figure 3). Second-mode waves are evident, with frequencies that rise as the boundary layer thins with increasing unit Reynolds number. Turbulence is apparent at some of the higher Reynolds number conditions. A turbulent spectrum exhibits elevated fluctuations at all frequencies, with no second-mode peak visible. An example of a turbulent spectrum is seen in Figure 3a at $Re/m = 13.3 \times 10^6$. Data from $x = 0.360$ m are plotted in Figure 3 because all of the types of waves that were observed were seen at that position. Data from $x = 0.208$ m and $x = 0.490$ m also show waves in multiple stages of growth, but waves were not visible for as many conditions at these locations. At $x = 0.208$ m, the waves are often too small to observe, and at $x = 0.490$ m, the flow has often become turbulent.

In the Langley Mach-6 tunnel, waves are observed at all tested Reynolds numbers on some but not all sensors. Transition appears on the PCBs for $Re/m > 6.66 \times 10^6$. It is inferred that transition has occurred when laminar spectra are evident on at least one sensor, but turbulent spectra are observed on sensors farther downstream. Linear waves are seen at the lowest Reynolds number condition, and larger, nonlinear waves at the next condition, showing growth with unit Reynolds number. At the rest of the conditions, the waves have saturated and begun to break down. The second-mode peak flattens out and disappears as the waves break down, and the low-frequency pressure fluctuations increase. In the late stages, the peak seems to be superimposed on a turbulent spectrum, and changes in amplitude are not evident at frequencies both higher and lower than the second-mode waves. The cause of the peak near 550 kHz is unknown.

In the Langley Mach-10 tunnel, waves are observed at all tested Reynolds numbers on at least some sensors. Transition is not observed on the PCBs in this tunnel, since a broad spectrum without a second-mode peak is not evident at the maximum unit Reynolds number.

The growth of the second-mode waves and their harmonics can be clearly seen as unit Reynolds number increases. The second-mode peaks increase in both height and width with increasing unit Reynolds number. Linear waves are present at $Re/m = 1.7 \times 10^6$, and a single harmonic has appeared by $Re/m = 3.4 \times 10^6$. For all subsequent conditions, three peaks are visible, indicating two harmonics.

In Tunnel 9, waves can be seen at $x = 0.360$ m from $Re/m = 2.2 \times 10^6$ to 13.5×10^6. A turbulent spectrum is seen at $Re/m = 30.2 \times 10^6$. Again, the waves at the lowest condition, seen near 125 kHz, are linear. At $Re/m = 3.8 \times 10^6$, the electronic noise level was elevated for an unknown reason. This run was the first run performed, and it was the only run to exhibit such elevated noise levels. However, the second-mode waves are still visible at about 200 kHz. The waves are nonlinear at the next condition, $Re/m = 6.5 \times 10^6$, with three peaks visible. At $Re/m = 13.5 \times 10^6$, the waves are still visible, but breakdown has begun. This is shown by the elevated low-frequency fluctuations, as well as the disappearance of the harmonics. A turbulent spectrum is observed at $Re/m = 30.2 \times 10^6$.

6 Calibration of PCB-132 Pressure Sensors for Measuring Second-Mode Waves

Berridge's work has recently focused on the development of a small high-quality shock tube for calibrating the PCB-132 sensors [16]. This 3-inch shock tube is a half-scale version of the well-established 6-inch shock tube at Caltech. Although the PCB-132 sensors have been very useful in a variety of wind tunnels, they are built and calibrated to measure the passage of shock waves. Second-mode waves are of much smaller amplitudes. Thus, the amplitude response and the spatial and temporal resolution of the PCB132's is not yet well understood. Improved estimates should be determined via specialized calibrations. These are to be carried out using weak shocks in the new shock tube. Under a nondisclosure agreement, Purdue is also now cooperating with PCB to help them develop improved versions of these sensors that are tailored for the measurement of high-frequency instability waves.

7 Support for Hypersonic Transition Collaborations within NATO RTO

The present AFOSR grant supported the author's work within NATO RTO AVT-136 (a Task Group supporting the Assessment of Aerothermodynamic Flight Prediction Tools through Ground and Flight Experimentation) and NATO RTO AVT-200 (a Specialist's Meeting on Hypersonic Laminar-Turbulent Transition, co-chaired by Prof. R. Radespiel and the present author). It also supported a fall 2011 visit by graduate student Amanda Chou to Germany. Amanda visited T.U. Braunschweig, where she spent two weeks learning about the T.U.B. laser perturber and how it relates to the Purdue laser perturber. She also visited the DLR in Braunschweig, Göttingen, and Cologne, helping to enhance collaborations between those four institutes and the Purdue effort. The DLR in Cologne plans an experiment in the Purdue Mach-6 quiet tunnel in June 2012, studying the effect of tunnel noise on the transition delay

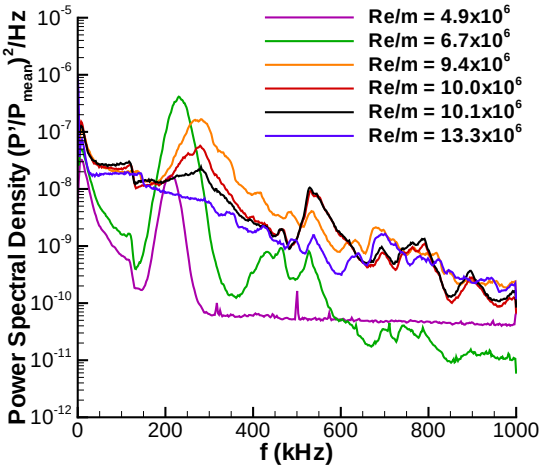

(a) Langley Mach 6, $x = 0.360$ m, $\phi = 0°$. Data for $Re/m = 4.9 \times 10^6$ is from $\phi = 120°$.

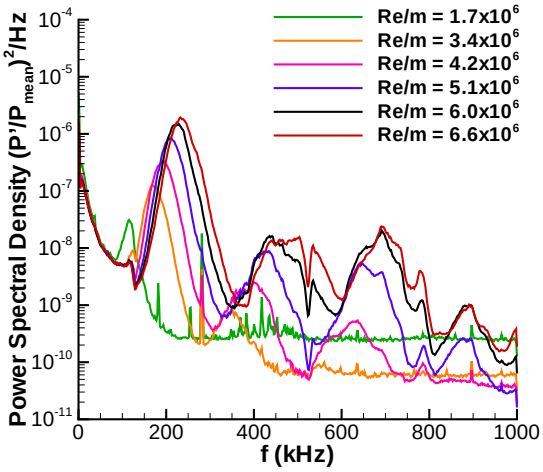

(b) Langley Mach 10, $x = 0.360$ m, $\phi = 0°$.

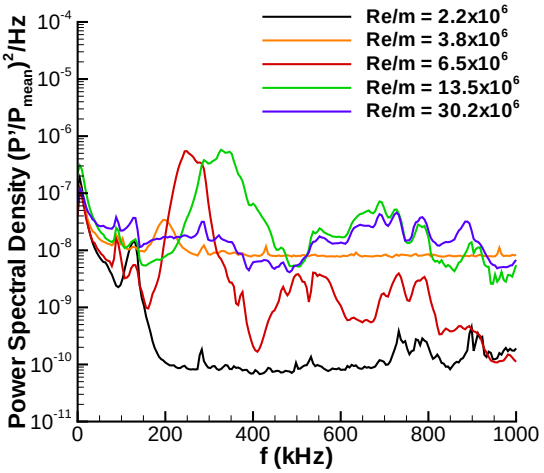

(c) Tunnel 9, Mach 10, $x = 0.360$ m, $\phi = 0°$.

Figure 3: PCB measurements on 7-deg. sharp cone at representative unit Reynolds numbers in three different tunnels.

generated by ultrasonic absorbing coatings, and has already been modifying their H2K model to work in the Purdue tunnel. The DLR plans to provide time in the large Mach-6 H2K tunnel in return, examining the transition reversal that occurs with larger nose radii on blunt cones.

8 Second-Mode Wave Packets and Turbulent Spots on the Mach-6 Nozzle Wall

8.1 Summary

Katya Casper has been measuring the pressure fluctuations induced by second-mode waves and turbulent spots, first on a cone and then in the thick boundary layer on the Mach-6 nozzle wall, where the frequencies are lower and easier to measure [22, 2, 11, 13, 17]. Casper has been supported by NDSEG and NSF fellowships and a Sandia internship. Her experimental measurements have been supported by Sandia and also the present grant. She designed a modular 7-deg. half-angle cone which was built with support from Sandia and also AFOSR, and operated at Purdue, Sandia, AEDC Tunnel 9 and NASA Langley. The second-mode wave amplitude at breakdown increased from about 5% at Mach 5 to 12% at Mach 6 and 24% at Mach 8 [22]. Since the tunnel noise also varies when the freestream Mach number varies, the cause of this marked variation is not yet known, but these results drew attention to the importance of nonlinear breakdown phenomena, since the amplitude at breakdown was clearly not constant. Her work on the pressure fluctuations and vibrations induced by a transitional and intermittently turbulent boundary layer is of interest to the Air Force as well as Sandia. Structural engineers at Sandia are collaborating with our group to help develop physics-based models for the temporal and spatial variations of the pressure-fluctuation field.

8.2 Research Highlights

Centerline and spanwise measurements have been made of pressure fluctuations beneath pulsed glow-induced disturbances at varying Re from $5.76 - 10.8 \times 10^6/m$. The spanwise measurements show the internal pressure structure of the disturbances during the growth and breakdown of wave packets into turbulent spots. A schematic of the experimental setup is shown in Fig. 4. A perturber is placed on the top wall of the tunnel at z = 1.924 m, where z is the axial tunnel coordinate measured from the throat. Downstream, there are various sensor locations along the tunnel centerline in a slender traverse plug insert. There is also a cylindrical pipe insert that was designed to fit between the nozzle exit and the diffuser sting support. When the tunnel is closed, the pipe insert fits flush with the nozzle exit and extends 0.254 m downstream. This pipe insert is actually made of five rings . One of the downstream rings has azimuthal sensor locations at y = $\pm$ 11, 21, 32, 42, and 63 mm. The four downstream rings are interchangeable to allow azimuthal measurements at any of the four downstream locations.

Fig. 5 shows ensemble-averaged centerline measurements at an intermediate Re of $8.25 \times 10^6/m$. At this Re, a second-mode wave packet with frequencies between 33 and 43 kHz

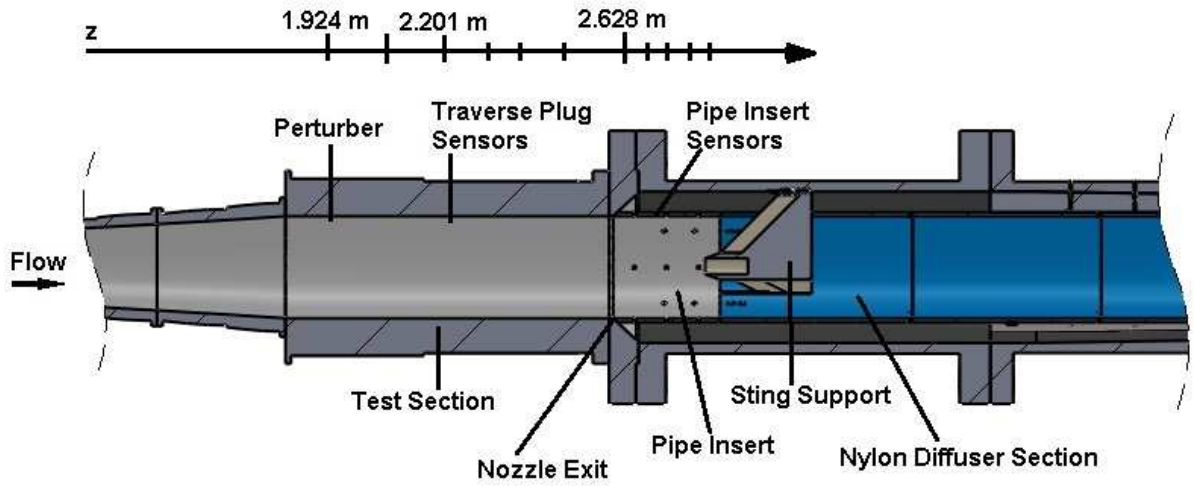

Figure 4: Schematic of experimental setup in the BAM6QT for nozzle-wall measurements. Perturber and sensor locations are marked on the z axis.

develops over the nozzle wall sensors. The frequency of the waves decreases as the boundary-layer thickens downstream. The wave packet eventually becomes nonlinear as indicated by the presence of harmonics in the PSD beginning at z = 2.480 m where a harmonic is seen near 76 kHz. This is farther upstream than the lower Re condition where nonlinearity became apparent at z = 2.679 m. The waves then become very large with positive fluctuations greater than p_∞ before they break down near z = 2.730 m. It is surprising that such large fluctuations are seen before the waves break down. Negative fluctuations remain much smaller and do not approach zero absolute pressure. The spectra of these large wave packets show many peaks in the spectra along with elevated broadband frequencies. Once breakdown occurs, the spectra show elevated broadband frequency components indicating the onset of turbulence in the boundary layer. Additional peaks in the spectra are no longer present. However, second-mode waves remain an integral part of the disturbance after breakdown. The waves are still seen at the front and rear of the disturbance. These residual waves appear as a broad peak in the spectra.

The pressure-fluctuation field within the disturbance as it breaks down into a turbulent spot is seen in contour plots at the four downstream measurement locations (Fig. 6). For the measurements at z = 2.679 m, the contour plot shows that the second-mode wave packet is still contained near the centerline. In the measurements farther downstream, the disturbance footprint still clearly shows the second-mode waves, but they have spread in the spanwise direction and become distorted. The spanwise edges of the wave packet are also jagged. By the measurements at z = 2.831 m, the spanwise spread of larger disturbances is evident and the characteristic arrowhead shape of the turbulent spots can be seen; however, it is unclear at which point the wave packet becomes a turbulent spot. There is a gradual change between the two cases. Breakdown of the waves occurs first on the centerline where the wave amplitudes are largest. However, traces of the second-mode waves can still be seen, especially at the front and rear of the disturbances as well as in the spanwise edges. Similar measurements were made at other Re between $5.76 - 10.8 \times 10^6/m$. As the Re increases,

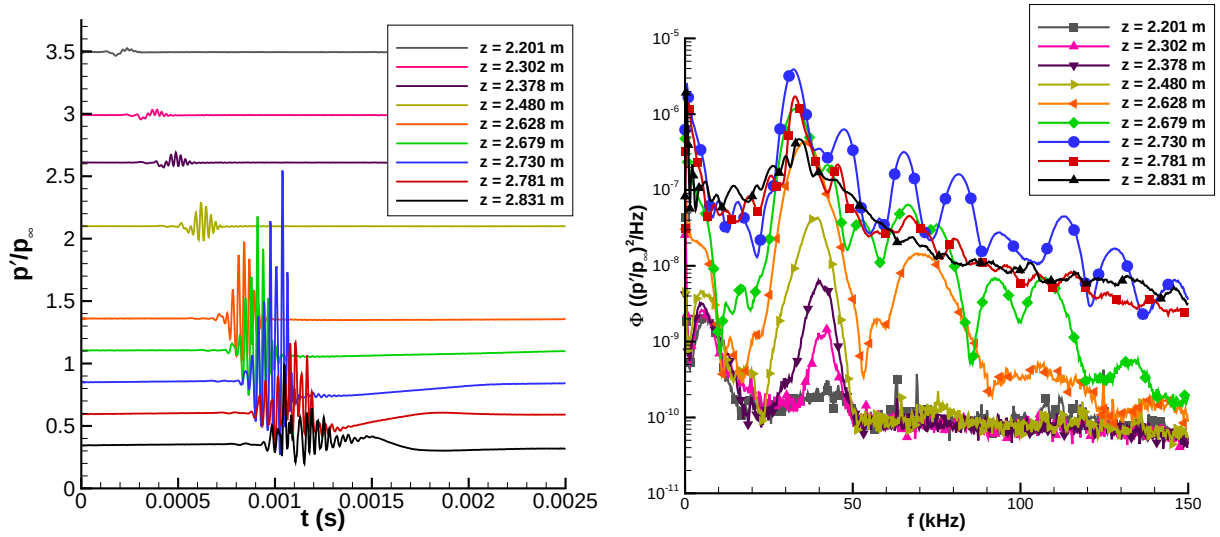

(a) (b)

Figure 5: Ensemble-averaged disturbances from spark perturbations, $Re = 8.25 \times 10^6/m$; (a) Pressure traces, each trace is vertically offset proportional to z; (b) Power spectral density.

the second-mode waves grow in amplitude sooner and break down to turbulence farther upstream. The spanwise extent of the wave packets and spots increases with Re and spreads farther in the spanwise direction.

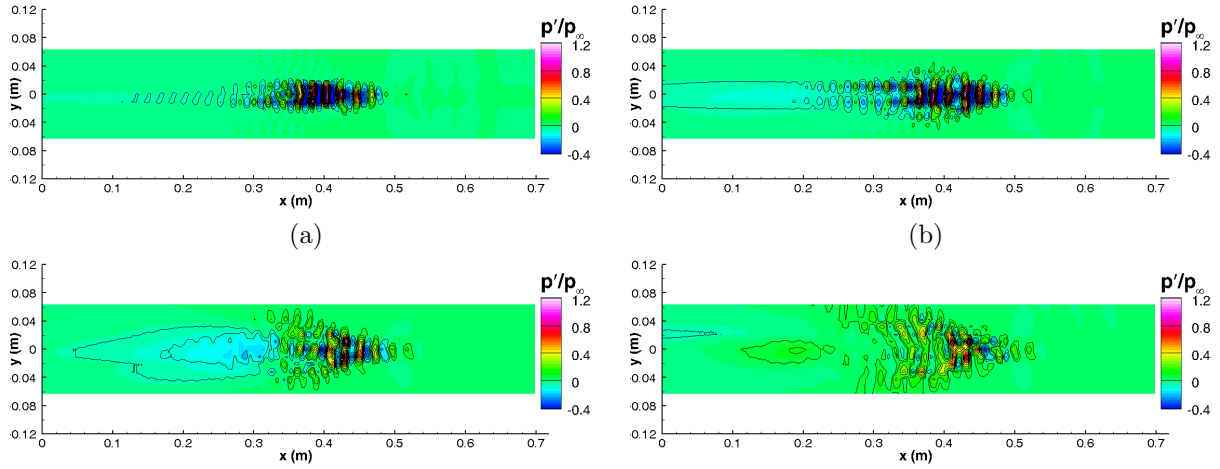

(a) (b) (c) (d)

Figure 6: Contour plots of spanwise measurements of ensemble-averaged disturbances, $Re = 8.32 - 8.34 \times 10^6/m$; (a) z = 2.679 m; (b) z = 2.730 m; (c) z = 2.781 m; (d) z = 2.831 m.

These measurements give a visualization of the growth and breakdown of spark-induced wave packets into turbulent spots. The spark perturbations initially generate small instability wave packets. The wave amplitudes grow with downstream distance and eventually become nonlinear, as indicated by the presence of harmonics in the spectra. The small wave packets are ordered and periodic. As they become larger, they distort and spread in the spanwise

direction. During the nonlinear growth, the waves can reach large amplitudes before breaking down to turbulence. Breakdown of the waves occurs first in the middle of the packet where the amplitude of the waves is largest. After breakdown, the central region of turbulence grows downstream and the typical arrowhead shape of the spots becomes evident. However, the second-mode waves remain an integral part of the disturbance; the waves are still seen in the front and in the 'calmed' low pressure region behind the spot as well as in the spanwise edges. As the spot progresses downstream, the turbulent portion of the spot grows larger in both the streamwise and spanwise directions. The second-mode waves are evident only at the periphery of the turbulence. Because of the gradual change from a wave packet to a turbulent spot, the location when a packet becomes a spot is still unclear. These results can be used to gain a better understanding of transitional pressure fluctuations in hypersonic boundary layers and can hopefully be used towards developing a turbulent spot model of the transitional pressure fluctuations.

9 Transition Induced by Very Large Second-Mode Waves on a Flared Cone

9.1 Summary

In 2008 it was already becoming evident that (1) second-mode waves could reach high and variable amplitudes before breaking down to turbulence, (2) in (nearly) all previous measurements of transition in quiet tunnels, only the front portion of the model was under quiet flow, so that the nonlinear breakdown of the instability occurred under noisy flow [31], (3) fairly complex axisymmetric models could be designed using stability analysis, specifically to achieve the highest possible instability-wave growth under quiet flow [38], (4) fairly complex axisymmetric models could be built on the 2001 CNC lathe in the department machine shop at a very affordable cost, (5) laminar flow seemed to extend past the nozzle exit in the Purdue facility, so the whole model could be studied at fairly high Reynolds number under fully quiet flow, and (6) it was desirable to generate very large second-mode waves under quiet conditions, so they could be measured with the new PCB-132 sensors [37]. Thus, it became both feasible and desirable to try to study transition due to large second-mode waves under fully quiet flow, using a specially designed model. Both Brad Wheaton and Tom Juliano became interested in this, and both designed highly unstable axisymmetric models for class projects in Fall 2008, using the Minnesota STABL code. Wheaton used a family of circular-arc geometries, and Juliano used a family of parabolic geometries [1]. A 1-mm nose radius was used for both geometries, to ease grid generation and model fabrication.

Both students developed flared-cone geometries that achieved very high N factors, which were near 17 under quiet tunnel conditions. Transition was expected near $N \simeq 10$, [39] so it was thought that suitable experiments could be carried out below the maximum quiet Reynolds number. Amanda Chou and Dennis Berridge then had the cone built for another class project, and tested it in Spring 2009. Surprisingly, (1) very large second-mode waves were observed under quiet flow, for the first time, and (2) the aft end of the cone was apparently still laminar, at the maximum quiet Reynolds number that was available at the time. Since the maximum computed N factors were near 20, this was very surprising.

Balakumar then computed the instability-wave growth to compare to the Purdue results [40], and found substantially smaller N factors, although they were still in the middle teens. Different settings were then used in the PSE marching procedure, to achieve better agreement between the STABL results and Balakumar's. Wheaton found that the maximum N factor was near 16 at the back of the model. This is primarily because the flared cone maintains a near-constant boundary-layer thickness over the whole model, so the same frequency is highly amplified over most of the cone. Local amplification rates are also somewhat higher due to the adverse pressure gradient, but this seems to be a secondary effect. Chou and Berridge measured wave amplitudes of 6-8% with no evidence of transition when the computed N factors were larger than 13. Under noisy flow, transition did occur, but at a surprisingly large N factor. However, the measurements from the PCB sensors were not all consistent, and further work was clearly needed. Since this topic was not a part of any existing student's Ph.D. thesis research, the work continued as a series of side projects.

Further progress was made in fall 2009 [7]. A new nosetip was fabricated for the same flared cone; with great care, the department machine shop was able to achieve a much smaller nose radius of about 0.16 mm on the needle-like nose. Even larger second-mode waves resulted, as expected. For the first time, temperature-sensitive paint measurements found streakwise streaks in the region where the large second-mode waves began to become turbulent. These streaks appear only under quiet flow, and are apparently associated with the nonlinear breakdown. The streaks appeared, weakened, and then strengthened again, a phenomena that was very surprising until it was explained in approximate DNS simulations by Fasel's group [41]. Under quiet flow, the cone remained laminar to N factors of at least 15 and perhaps as high as 19. Transition occurred under noisy flow at $N = 9$, which is also surprising.

The June 2010 paper reported initial efforts to control the streamwise streaks using small roughness dots [10]. Changes in the dot spacing were able to induce changes in the spacing of the streamwise streaks, and more sensors were installed on the cone. Transition appeared to occur at $N \simeq 18$ under quiet flow. Further improvements in measurement technique were clearly desirable, along with improvements in methods for applying small triggering roughness.

Further progress was then reported in June 2011 [15]. Transition seemed to occur at the very downstream end of the cone, at a total pressure of 163 psia. However, efforts to obtain natural transition under unambigously quiet flow were not yet successful. Ryan Luersen took over this project, and applied small roughness dots using a microsyringe with epoxy, a new technique. Similar results were again observed but improved measurements remained necessary.

The most recent report is from Jan. 2012 [16]. A longer flared cone was successfully built and started successfully. Improved methods were developed for painting the cone and applying small roughness arrays. Once again, the streamwise streaks appeared under quiet flow, weakened, strengthened, and this time clearly transitioned before the end of the cone, apparently under quiet flow. Rolling the cone showed the streaks were fixed to small roughness on the body.

Ryan Luersen plans to perform additional experiments in this area for his M.S. thesis, expected August 2012, after which Ryan is to leave Purdue. A new student has been recruited to continue the work in 2013. Flared cones of this type show great promise for studying the

nonlinear breakdown of second-mode waves into turbulence. They do suffer from some factors that are not common in applications: (1) Görtler vortices that may influence the nonlinear breakdown, and (2) the same frequency is amplified over a long distance, which is not likely to occur in general. However, they do permit the generation of second-mode-induced transition under fully quiet flow, at least in the Purdue tunnel, apparently. In addition, the models are not expensive to build. Plans thus call for continued studies of geometries of this general type.

9.2 Research Highlights

The flared cone geometry has presented a unique platform for studying a nonlinear transition process in a hypersonic boundary layer. The flare of the cone maintains a nearly constant boundary layer thickness after the region of initial boundary layer growth, causing continuous amplification of second-mode waves in a narrow frequency band. These waves have been shown to reach N-factors up to 17 near the rear edge of the cone. [26]

The transition process creates a set of streamwise streaks of increased heating followed by a decrease in heating to near-laminar levels. At high enough Reynolds number there is a second increase in heating, and pressure fluctuation measurements indicate that the flow begins transitioning to turbulence. It has been hypothesized that this complicated process is due to interactions between the second-mode waves and streamwise vorticity, possibly as a result of the Görtler instability. [42] Fasel, et al. used DNS to show streak heating behavior due to nonlinear second-mode wave growth that resembles what has been seen in experiments.[43, 41] Sivasubramanian and Fasel state, "The first peak in the skin friction roughly corresponds to the streamwise location where the primary wave saturates. As the primary wave starts to decay following the nonlinear saturation, the skin friction decreases strongly. Then finally, a steep rise in skin friction occurs when all higher modes experience strong nonlinear amplification..."[43]. Here the primary wave is at the most amplified frequency, and the skin friction is considered to be proportional to heat transfer.

Streamwise vorticity has also been introduced via small roughness elements placed on the cone, and a similar transition process has been observed. [26] However, the size and spacing of these roughness elements were not well controlled, so several methods for improving control are currently being investigated.

With the original flared cone model, transition could be seen at the rear of the model only at stagnation pressures above 160 psia. [15] The high pre-run pressure in the test section necessitated the use of two small port-hole windows for TSP image acquisition, instead of the larger rectangular window, which is only rated to 152 psia. The porthole windows limit the field of view on the model, which makes it difficult to obtain an image of the full transition process. Therefore, a longer flared cone model was fabricated that could achieve sufficiently high Reynolds number for transition, at a stagnation pressure that is low enough to allow the use of the rectangular window. The new model has the same flare as the old model, but it is 3-in. longer, which allows more of the transition process to be seen using the rectangular window at lower stagnation pressures. The longer model also increases the maximum attainable quiet Reynolds number by approximately 15 per cent. The data presented herein were obtained using the new, larger cone at a stagnation pressure of approximately 140 psia.

Figure 7 shows the cone's characteristic transition process, as described above. Sensors were not yet installed on the cone, so no heat transfer data is available. A streamwise temperature profile is plotted in Figure 8. This profile was taken along a ray approximately 6.5° below the centerline and it runs through the center of a streak. The shape of this profile is typical, but the absolute values of the temperatures vary from run to run. In this case, the maximum temperature change in the streak (at approximately 16-in.) is roughly three times greater than the temperature change in the laminar region upstream of 13.5-in. and it is roughly equal to the temperature change in the transitional region downstream of 19-in.

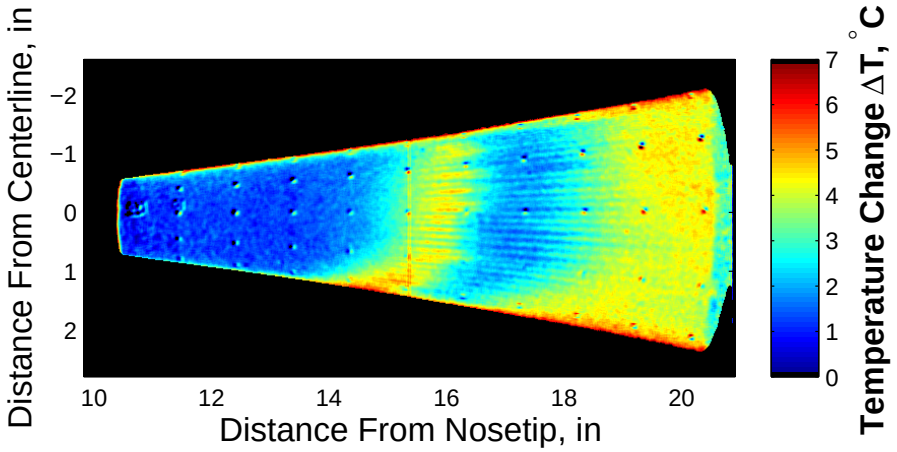

Figure 7: Typical TSP image at a stagnation pressure of 140 psia.

The temperature profiles at a fixed axial location are plotted in Figure 9 for two runs that were done back to back with the same cone orientation, and these two baseline cases repeat fairly well. The orientation of the cone can be identified by the fiducial mark that can be seen just above the centerline registration mark (the small black dot) at $x = 11.5$ in. in Figure 7. The fiducial mark is the number "01," which appears blurry in TSP images, but can be clearly seen in the raw pictures.

The cone was rolled up and down by 30° relative to the baseline orientation to determine whether the streaks are body-fixed. Figure 10 shows a typical temperature profile from each orientation, plotted in body-fixed coordinates relative to the fiducial mark. The temperature profiles were also normalized by their respective maximum temperatures for ease of viewing. It's clear that the streaks line up, indicating that they originate with small roughness features on the cone's surface, rather than freestream disturbances.

The average angle between temperature peaks for the data plotted is shown in Table 1. Averages over each run were calculated over 14 streaks for the baseline cases (fiducial mark on window centerline), and 7 streaks for the rolled cases (fiducial mark ± 30° from the centerline). Streak widths and standard deviations (STD) of streak widths are rounded to the nearest tenth of a degree, and wavenumbers are rounded to the nearest integer.

The streak widths are consistent from run to run for each configuration, and the variation in streak widths across the three configurations is roughly 10 per cent. Again, this indicates

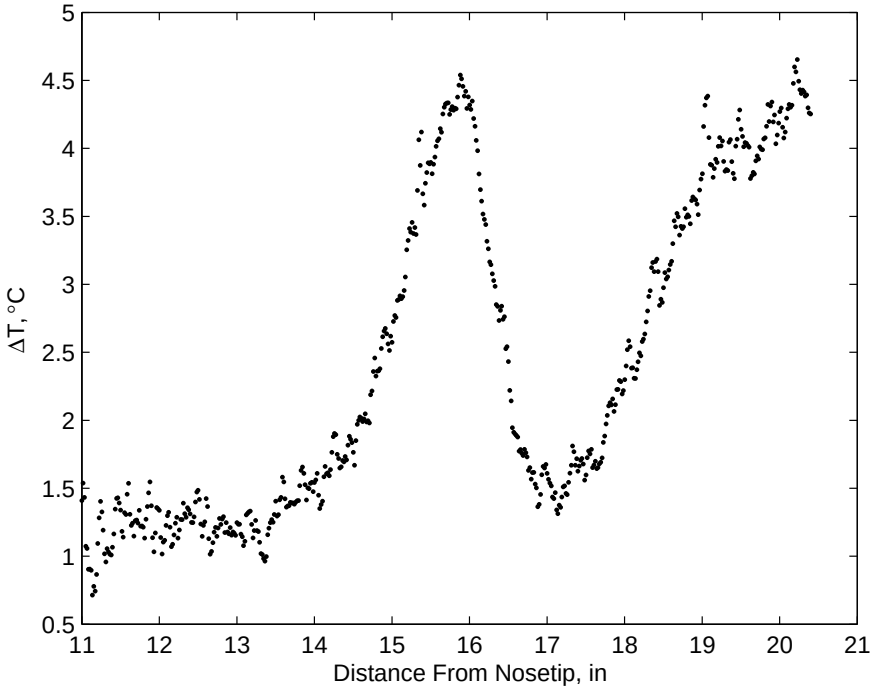

Figure 8: Temperature change along a ray.

that the streaks are induced by natural surface roughness, and therefore can be controlled through the application of roughness elements.

Table 1: Average Streak Separation and Wavenumbers

Orientation	Streak Width	STD of Streak Width	Wavenumber
Centerline	4.8°	1.1°	76
Centerline	4.8°	1.1°	76
30° down	5.0°	1.1°	72
30° down	5.0°	1.3°	72
30° down	4.9°	1.4°	74
30° up	4.5°	0.9°	80
Average	4.8°	1.1°	75

10 Instabilities in the Wake of an Isolated Roughness on the Mach-6 Nozzle Wall

10.1 Summary

Roughness often plays a role in the instability processes that lead to transition under various conditions [44]. Isolated roughnesses are less difficult to study, since they generate a

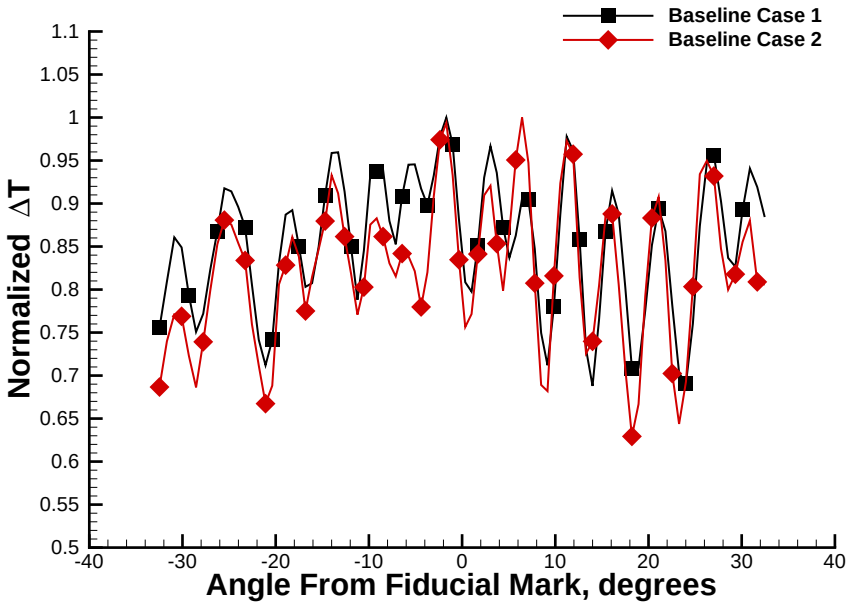

Figure 9: Spanwise Temperature Profiles

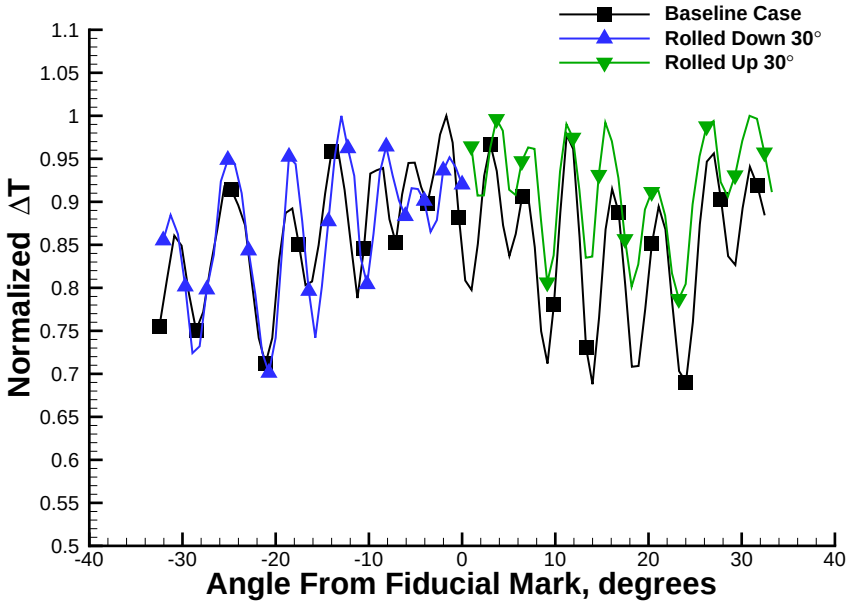

Figure 10: Spanwise Temperature Profile on Cone at Different Roll Angles

wake within the boundary layer which creates new instabilities that may cause transition to turbulence. The thick (1-cm) laminar boundary layer on the nozzle wall of the Mach-6 quiet tunnel generates relatively low frequencies and large spatial scales when an isolated roughness is inserted [14, 23]. Brad Wheaton has been measuring the instabilities in the wake of a cylindrical roughness in this boundary layer, comparing to computations by U. Minnesota, NASA Langley and others. Although this work was initially funded by a NASA cooperative agreement, and then in part by the NASA Constellation University Institutes Project (CUIP), and now in part by a short-term partial extension of CUIP, partial AFOSR funding is enabling Wheaton to complete his Ph.D. in this area in an orderly fashion. Wheaton has obtained the first measurements of instabilities induced by an isolated roughness in a hypersonic boundary layer, with successful although incomplete comparisons to computations by Bartkowicz at U. Minnesota. He is now studying reduced roughness heights that are just sufficient to induce transition well downstream, and is to compare to computations by Choudhari et al. at Langley. He shares a downstream nozzle-wall measurement apparatus developed by Casper with funds from Sandia.

10.2 Research Highlights

Because the instability originates in the separation region upstream of the roughness, surface-pressure data were analyzed from both experiment and CFD at $x/D = -2.0$ and $x/D = -1.5$ [14]. Power spectra are plotted for both locations upstream of the roughness, as well as from experimental data taken in the absence of the roughness with a laminar and turbulent boundary layer (Figure 11). The experiments were performed from runs with an initial stagnation pressure $p_{0,i} = 95$ psia and a stagnation pressure of $p_0 = 90$ psia, to match the stagnation pressure in the Minnesota computations by Bartkowicz et al. The legend in Figure 11 shows the RMS pressure (taken from integrating the frequency range of the instability peaks) nondimensionalized by the mean surface pressure. The frequency resolution of the spectra is 0.25 kHz for the experiments and 1.25 kHz for the CFD. Both the experiment and the CFD show the main peak for the instability, which occurs near 21 kHz for the experiment but at a slightly lower frequency of 18 kHz for the CFD. It is possible that the frequency is lower because the grid is not adequately resolved. Both experiment and CFD show several harmonics, which are more clearly visible at $x/D = -1.5$. At $x/D = -2.0$ the experimental spectrum appears to have a lower peak amplitude but with fluctuations that are more broadband. The instability amplitudes show good agreement (2.7% vs. 1.9% at $x/D = -2.0$ and 6.6% vs. 6.4% at $x/D = -1.5$ for the experiment and CFD, respectively). At both sensor locations, the spectra are already near smooth-wall turbulent fluctuation levels even upstream of the roughness. It is unclear if this flow could be classified as turbulent solely due to these high fluctuations; large peaks from the instability still remain in the spectra.

The experiments and simulation have together identified the apparent mechanism for transition due to this large isolated roughness. The core flow of the wind tunnel is Mach 6 which means that a separation shock is created by the displacement of the separation bubble. This separation shock meets the bow shock formed from the roughness element extending into the flow and creates a λ-shock. Behind this bow shock is a large increase in pressure. This high pressure 'pushes' the flow down towards the tunnel wall where it gets entrained back into the separation bubble (Figure 12). Unsteadiness created in this

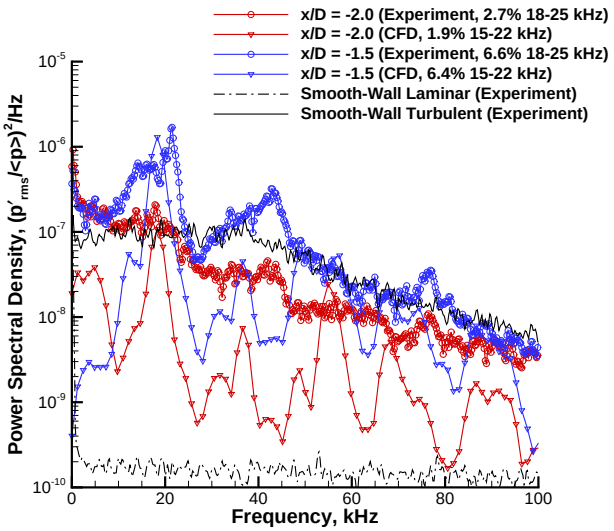

Figure 11: Power spectra from two sensors upstream of the roughness (both experiment and CFD).

region is the mechanism for transition downstream and it is worth noting that this situation is very similar to the spike-tipped body instability. There are essentially two stages in the unsteadiness: an inflationary stage and a collapsing stage. In the inflationary stage, flow behind the bow shock becomes entrained in the separation region. This causes the primary horseshoe vortex to grow while pushing the separation shock upstream. Due to the separation shock moving upstream, the normal shock weakens and pushes less fluid back into the separation region. This begins the collapsing stage in which the vortex shrinks and the separation shock moves closer to the roughness again, strengthening the bow shock and beginning another inflationary stage. The result is a 'breathing' of the separation bubble which creates disturbances that are sent downstream.

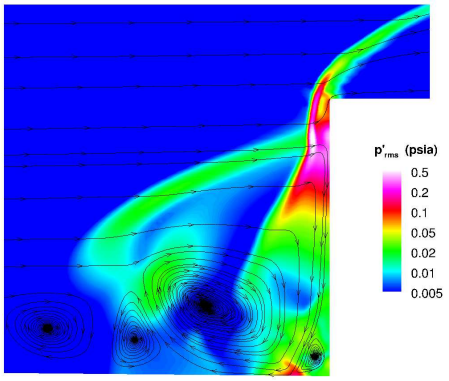

Figure 12: Contours of RMS pressure along the centerplane upstream of the roughness, showing the oscillating shock structure and separation bubble. Streamlines are also plotted.

11 Further Characterization of the Flow Quality in the Mach-6 Quiet Tunnel

Flow quality in a hypersonic quiet tunnel is not easy to characterize, since in addition to the usual concerns about flow uniformity and angularity, it is critical to determine the freestream perturbations and their dependence on tunnel conditions. Although the short run time of the Mach-6 Ludwieg tube reduces operating costs and improves efficiency, it does make it more difficult to generate a survey of the freestream flow quality.

Laura Steen made numerous measurements of the freestream flow quality for her M.S. thesis [25], in addition to aiding with the development of the new stainless-steel nozzle throat (which is not yet complete). A summary of her results appeared in Ref. [10]. Remarkably, for the first two seconds of quiet flow, the pitot pressure fluctuations are about 0.01% of the mean pitot pressure, everywhere in the nozzle where they have so far been measured. However, they then increase, but only for locations sufficiently far downstream within the nozzle. It seems that at later times, the nozzle-wall boundary layer transitioned near 75 inches from the throat [25, Fig. 4.17]. This occurred at 90 psia stagnation pressure, which is relatively low due to the problems with nozzle-throat finish that were occurring during most of Steen's measurements. The increase near 2 sec. may be caused by increased disturbances passing through the nozzle throat [45].

It has been suggested that when the air is not suctioned over the bleed lip and a turbulent boundary layer is generated by the bleed lip serving as a trip, the BAM6QT may be noisier than conventional wind tunnels. To check the noise generated by the closed bleed slot, a Kulite-pressure-transducer pitot probe was run twice, above the BAM6QT maximum intermittently-quiet pressure, once with the bleed slot open and once with the bleed slot closed. For these runs, the BAM6QT maximum intermittently-quiet pressure was near 160 psia. At high pressures above 200 psia, the nozzle-wall boundary layer is fully turbulent whether the suction slot is open or closed. For these tests, the RMS noise levels were calculated for 0.1-second intervals and normalized by the mean pressure. Steen's results are shown in Figure 13a, plotting RMS/mean against the falling stagnation pressure.

Since the noise levels are nearly identical for both cases, it seems that any air circulating around the bleed lip under noisy flow has little to no effect on the pressure fluctuations. The noise radiated from the turbulent boundary layer near the nozzle exit is apparently unaffected by the bleed slot 7 feet upstream. A comparison of the power spectral density for these two runs is also shown in Figure 13b. This plot shows that the power spectral densities for these two runs were nearly identical. These two spectra were taken for the same time and stagnation pressure during each run. Of course, tunnel noise varies with Mach number, unit Reynolds number, nozzle size, and so on, so different conventional tunnels have different noise levels [46].

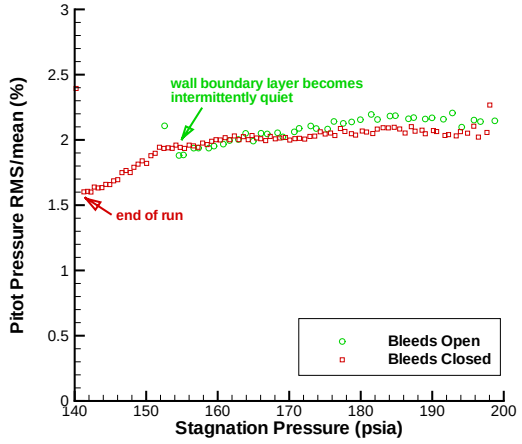

(a) RMS fluctuations

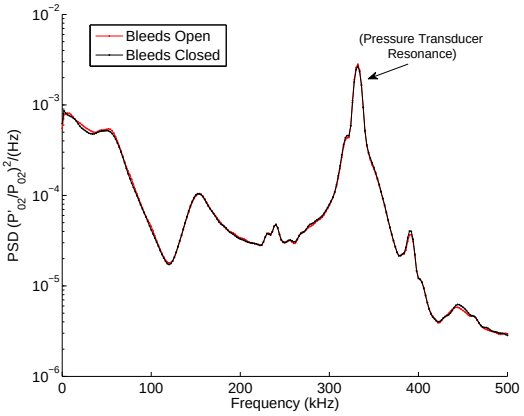

(b) Power Spectral Density of RMS fluctuations. $t = 0.4$ seconds and $P_0 = 196$ psia for both runs

Figure 13: Kulite pressure transducer probe positioned at z=84.9 in. downstream of the throat along the centerline, just upstream of the test section. For the suction-slot-open run, the nozzle-wall boundary layer becomes intermittently quiet at approximately 155 psia. For the suction-slot-closed test, the run ends at approximately 140 psia.

12 Adapting the Laser Perturber to the Mach-6 Quiet Tunnel

Schmisseur and Salyer developed a laser perturber for introducing controlled perturbations in the freestream ahead of a bow shock [47, 48, 49]. In March 2007, Tumin and Fasel from Arizona and Zhong from UCLA wrote a white paper with the present author, agreeing on an ad-hoc coordinated effort to study receptivity on circular cone at zero angle of attack at Mach 6, using this perturber. Amanda Chou began her graduate studies in August 2008, focusing on this area, although she also spent a significant fraction of her time working with the flared cone [26]. The laser-perturber apparatus is complex, expensive, and not easy to operate, so it has taken some time to adapt it to the Mach-6 quiet tunnel.

The original Nd:YAG laser cost $63K in Dec. 1993. Since newer lasers are not substantially better for this application, and since the budget was limited, this laser was resurrected for the Mach-6 tunnel work. It provides about 230-300mJ/pulse at 532nm and 10Hz, so it is not trivial to learn to use it safely. After six years without being used, it was also necessary to get it repaired and adjusted, which cost about $10K in Fall 2008. The laser was moved to a newly procured rolling optical bench, so it could be operated with a test cell in Room 29A or under the Mach-6 tunnel in Room 29B. Power was installed in both locations. Chou's Dec. 2010 M.S. thesis describes her efforts to become familiar with the laser and its operation, and to reproduce in a new test cell the photoionization experiments from the 1990's. A tightly-focused beam is essential to generating the photoionized hot spot in low-density air with a limited-energy beam.

It was then necessary to design optics to generate the tightly-focused beam in the Mach-

6 tunnel. Fortunately, both flat and conformal windows were available for this purpose, having been provided by AEDC as part of a Phase III SBIR to Metrolaser ca. 2002. Prof. Collicott worked to design a new set of optics, although there was very little funding to support this effort. He designed an optical system for the Mach-6 quiet tunnel in August 2010 [12, 26], and the parts were then procured and assembled. Unfortunately, this system was found to have an unacceptable amount of astigmatism when used in conjunction with the contoured Mach-6 tunnel windows, resulting in a system that was not able to produce laser-induced breakdown plasmas in a test cell, even at atmospheric pressure. Because of this, the contoured window and compensating optical element were removed and the system was tested using the flat window that fits the Mach-6 tunnel. This system appeared to work about as well as the optimized Mach-4 system. However, since the flat window must be used, the nozzle-wall contour is more flawed, and undesirable aerodynamic characteristics could result. Measurements are still being made to test the effect of the flat window on the flow, although early results look promising. Measurements of the perturbation characteristics in a test cell are also still in progress.

13 Resonance in a Forward-Facing Cavity

13.1 Introduction

A forward-facing cavity was also tested in the Mach-6 tunnel [16], to once again serve as a simple initial test case for the use of the laser perturbation system [50, 51]. For the first experiments, the cavity was run without controlled perturbations. The new measurements found a critical depth for the forward-facing cavity near $L/D = 1.2$, in the first clearcut measurement of this type. This geometry may yet find application for use with heat-seeking missiles.

The forward-facing cavity was originally used as a passive method of reducing the stagnation point heat flux for high-speed missiles. Dynamic pressure measurements within the cavity showed that the forward-facing cavity resonated and that the bow shock oscillated at the same resonant frequencies. Cavity oscillations are always large under conventional noise. Ladoon et al. [50] showed experimentally that these oscillations exist in low-noise environments as well. The oscillations are small under quiet flow for shallow cavities.

At some critical depth, self-sustained resonance of the cavity occurs, where noise is damped very little or not at all. Ladoon [50] attempted to find this critical length in the Purdue Quiet Flow Ludwieg Tube (Mach-4 Tunnel) using a controlled laser perturbation. Ladoon ran experiments with and without a controlled perturbation but found that his maximum possible cavity depth was too short to study the critical depth characteristics. Using extrapolation, Ladoon calculated the critical depth of the cavity to be about $L/D = 2.7$. Segura [52] used a model with a longer maximum possible cavity length of $L/D = 3.0$ in the same tunnel and found self-sustained resonance at cavity depths greater than $L/D = 1.3$. Ladoon and Segura found that the cavity was very sensitive to the presence of freestream disturbances and that the amplification of these disturbances increases with the cavity depth. Numerical simulations by Engblom, et al.[53] showed that shorter cavity depths require some freestream noise to cause resonance. For longer cavity depths, resonance was obtained with

little or no freestream noise.

Experiments and computations have found that the primary resonant frequency for the forward-facing cavity is that of a standing wave in a resonance tube. This resonant frequency is given by the expression:

$$f_{1n} = \frac{\omega_{1n}}{2\pi} = \frac{a_0}{4L^*} \tag{1}$$

where a_0 is the speed of sound within the cavity and $L^* = L + \delta$ is the adjusted cavity depth. L is the depth of the cavity and δ is the average bow-shock stand-off distance. The flow velocity in the cavity is assumed to be small so that the stagnation temperature can be used to estimate the speed of sound. A bow-shock stand-off distance of $\delta/D = 0.24$ can be used for the forward-facing cavity. [52] This is an approximation, using a value between that of the shock stand-off distance of a three-dimensional cylinder with a flat nose and that of a hemisphere.

13.2 Model and Instrumentation

A forward-facing cavity model designed by Rodrigo Segura [51] was used in the BAM6QT (Figure 14). The model is a hemisphere with 19.05 mm radius and a 19.05-mm-diameter circular cavity. The depth of this cavity is adjusted via a cylindrical steel insert, which can be slid forward or aft in the cavity and secured with set screws. The maximum depth of the cavity is about $L/D = 5.00$, or 95.25 mm. One B-screen Kulite XCQ-062-15A pressure transducer was mounted in the center of this steel insert. Since the Kulite was mounted in a "pitot configuration," or facing directly into the flow, a B-screen Kulite was used to protect the sensor from particle impact. Each cavity depth was run in quiet flow, then again in noisy flow, at an initial stagnation pressure of 1114.2 ± 3.4 kPa and an initial stagnation temperature of 159.6 ± 5°C. The uncertainties in these conditions are simply the variation between each of the runs.

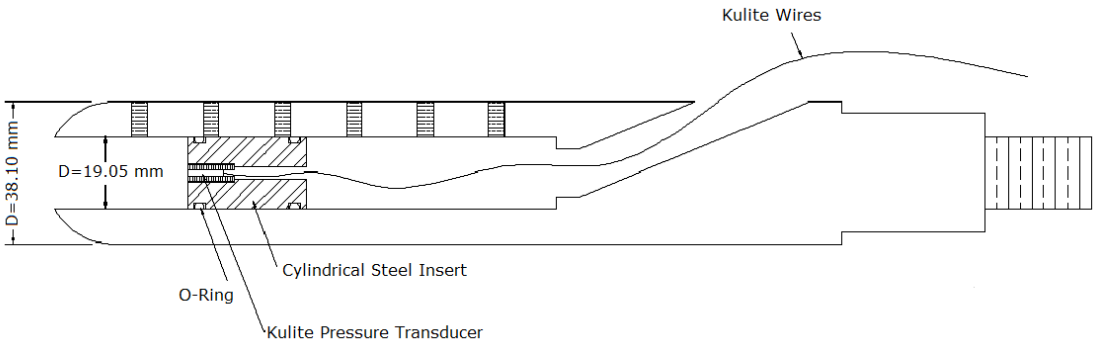

Figure 14: Schematic of forward-facing cavity model.

13.3 Fluctuations Induced by Freestream Perturbations

Different cavity depths from $L/D = 0$–5.00 were tested. Time traces for a shallow cavity (black trace) and a deep cavity (red trace) are given in Figure 15. The blue trace in Figure 15

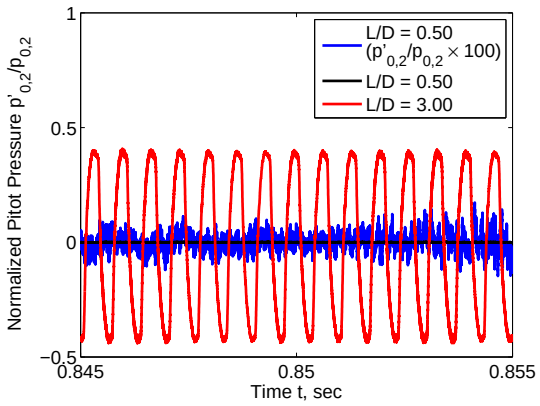

Figure 15: Time trace of shallow cavity (black trace) and deep cavity (red trace) in quiet flow.

is the black trace magnified 100 times to better show the pressure fluctuations measured at the same condition. Very little resonance is exhibited by the short cavity. While there may still be some resonance of the shallow cavity, a cavity will not be considered to be "self-resonating" in this paper unless the amplitude of that resonance is significant compared to pitot-pressure fluctuations under the same conditions. A significant amplitude of resonance is determined by comparing the normalized RMS amplitudes of several different cavity depths with measurements of freestream noise with a pitot tube.

Since the Kulite pressure transducers are mechanically stopped at pressures above 15 psia, they do not provide readings at full stagnation pressure. Therefore, traces were taken at vacuum pressure with no flow to find the spectra of the baseline electronic noise. The root-mean-squared spectra of the two different cavity depths at the same condition and a vacuum trace are given in Figure 16. Power spectra are computed for 0.1-second samples using Welch spectral estimation and Blackman windows. Fast Fourier transforms (FFTs) of 0.2-second segments with up to 50% overlap were taken and averaged together to form the power spectrum. A table of calculated RMS values and the frequency band used for integration is provided in Table 2 The resonant frequency is measured as a peak near the expected organ-pipe frequency. The black trace in Figure 16 corresponds with a cavity depth of $L/D = 0.50$, where there should be no self-sustained resonance. There is, however, a peak at around 6 kHz, which is the cavity depth's expected resonant frequency. This is considered a weak resonance of the cavity, but not a clear self-sustained resonance. The red trace corresponds with a cavity depth of $L/D = 3.00$, where there is a clear self-sustained resonance. This is shown by the large fundamental peak at about 1.5 kHz and the presence of large harmonics of the fundamental frequency. The presence of these large, sharp peaks indicates large amplitudes of sinusoidal frequency content. The RMS amplitude of the fundamental peak is about 31% of the mean pitot pressure ($p'_{0,2}/p_{0,2} = 0.31$), which is about four orders of magnitude larger than the pitot-probe trace.

Figure 17 shows the measured fundamental frequency for various cavity depths and compares them to the expected theoretical values. At shallow depths, where $L/D < 1.00$, the measured fundamental frequency differs from theory by 9–21%. For deeper cavities, where $L/D \geq 1.00$, the measured fundamental frequency differs by 9–11% from theory. Noisy flow

Table 2: RMS amplitudes for selected cavity depths in quiet flow

L/D	Frequency Band for Integration (kHz)	RMS/mean $(p'_{0,2}/p_{0,2})$
Pitot Probe	6.16–6.87	1.57×10^{-5}
0.50	6.16–6.87	1.82×10^{-4}
3.00	1.46–1.56	0.308

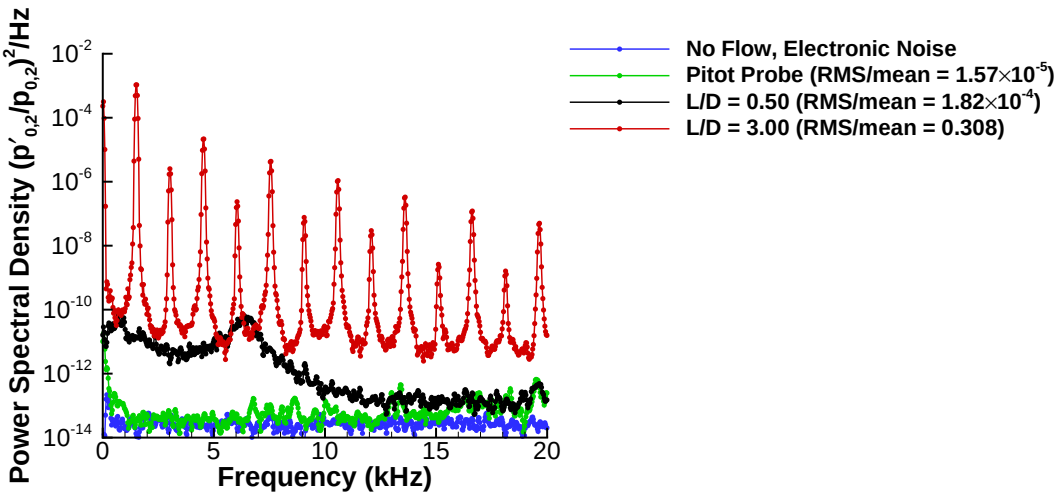

Figure 16: Effect of cavity depth on resonant frequency measured.

measurements of the fundamental frequency differ from quiet flow measurements by 5.6% at most. This indicates that the measured resonant frequency agrees fairly well with theory for deep cavities. The small discrepancy between the measured and theoretical fundamental frequency could come from the estimation of the bow-shock stand-off distance.

The measured pressure fluctuations are normalized by the measured mean pitot pressure. The root-mean-square of the pressure fluctuations is calculated by taking a power spectra of the normalized pressure fluctuations, integrating the power spectra of the fundamental peak across the full width at half the maximum value, and then taking the square root of this integral. These data are given in Figure 18. Figure 18a shows shallower cavities ($L/D < 1.5$) with the vertical axis expressed on a logarithmic scale. Typical pitot-probe measurements of freestream noise on the centerline at similar conditions are shown by a gray dashed line for quiet flow and a gray dash-dot line for noisy flow. The RMS pressure fluctuations for the pitot-probe measurements are taken by integrating across 6.16–6.87 kHz. This is the same range of frequencies used to find the RMS pressure fluctuations for $L/D = 0.50$. The noise level for the pitot-probe measurements is one order of magnitude less than similar measurements made by Steen. [25] This is because Steen integrated from 0–60 kHz to find the RMS pressure fluctuations. Noisy flow data are in red circles and quiet flow data are in blue squares. RMS fluctuations for deeper cavities, where $L/D > 1.0$, are presented on linear axes in Figure 18b. The pitot-probe measurement of freestream noise is not presented in this graph because it would be indistinguishable from the horizontal axis at this scale.

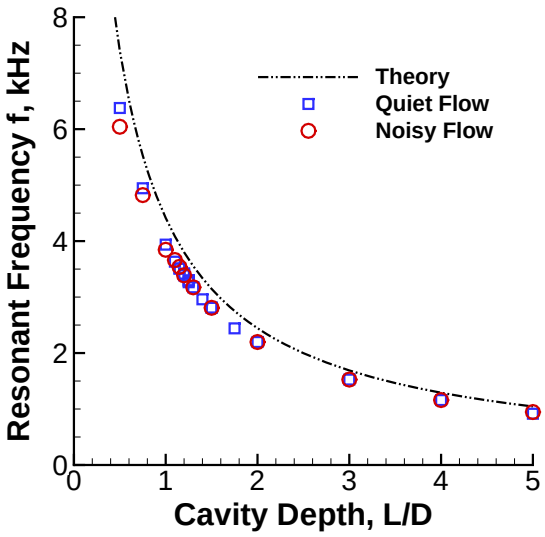

Figure 17: Effect of cavity depth on resonant frequency measured.

The noisy flow data are again shown by the red circles and quiet flow data are shown by the blue squares.

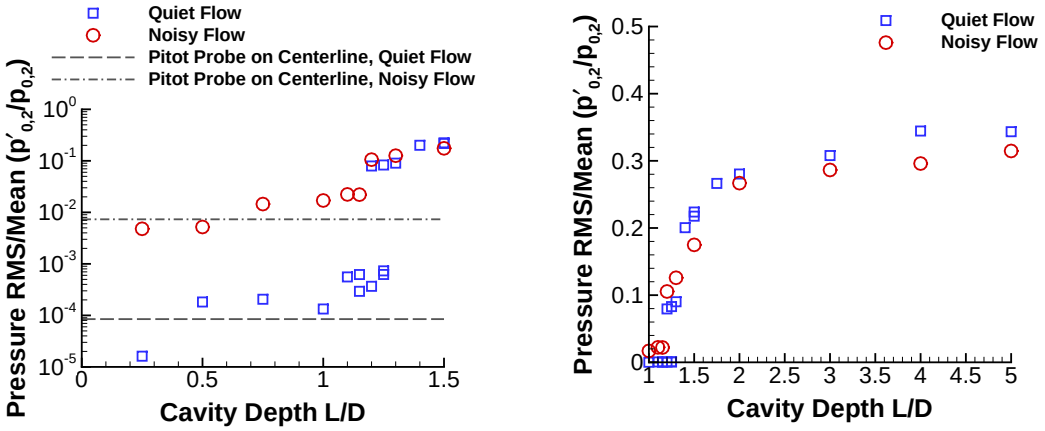

(a) Shallower cavities: $0 < \frac{L}{D} < 1.5$ (semi-log scale)

(b) Deeper cavities: $1.0 < \frac{L}{D} \leq 5.0$

Figure 18: Change in normalized RMS pressure fluctuation with change in cavity depth.

The RMS pressure fluctuations appear to be similar to the pitot-probe measurements of freestream noise for cavity depths up to $L/D = 1.15$. At $L/D \geq 1.15$, the fluctuations measured in the forward-facing cavity in quiet flow are about the same in magnitude as those of the noisy-flow fluctuations. At these depths, the quiet flow RMS pressure fluctuations increase by at least two orders of magnitude. At shallower cavity depths ($L/D \leq 1.15$) the noisy-flow RMS pressure fluctuations are higher than in quiet flow, which is expected. However, it is interesting to note that for deeper cavity depths, where self-sustained resonance occurs, the noisy-flow fluctuations are slightly lower in magnitude than those under quiet

flow. The reason for this is unknown. It is possible that three-dimensional fluctuations break up the resonance and therefore cause lower-magnitude pressure fluctuations in the cavity.

13.4 Fluctuations Induced by Noise Radiated from Passage of Turbulent Spot on Nozzle Wall

A Sentex hot-film array mounted on the BAM6QT nozzle wall shows a turbulent spot (blue trace in Figure 19). The forward-facing cavity, which was not previously experiencing self-sustained resonance, shows the effect of this turbulent spot on the model. The red trace in Figure 19 represents the damped resonance created by the Mach wave radiated from the turbulent spot on the nozzle wall. This uncontrolled experiment is similar to the controlled laser-perturbation experiments previously done by Ladoon et al. [50]

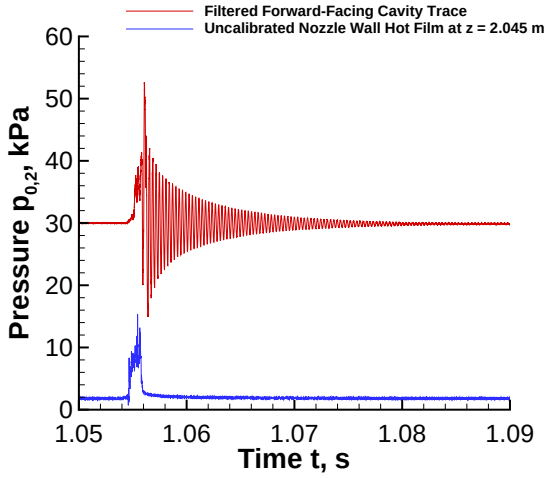

Figure 19: Effect of a turbulent spot on cavity resonance. $L/D = 1.15$, $p_0 = 1018.4$ kPa, $T_0 = 420.5$ K.

14 Crossflow Instability on a Cone at Angle of Attack

To study the effect of the crossflow instability on boundary-layer transition, experiments were performed on a 7-deg half-angle cone at 6-deg angle of attack with temperature-sensitive paint [27]. The first set of experiments looked the effect of tunnel noise on the crossflow instability. The results showed a significant effect of tunnel noise on the crossflow instability. Under quiet flow, the stationary vortices were visible but did not break down to turbulence. Under noisy flow, the stationary vortices were not visible, and transition occurred [6]. On a 6% blunt cone in noisy flow, transition began on the yaw side, an indication of crossflow-induced transition. Early attempts at influencing the crossflow instability using arrays of roughness dots yielded mixed success [6].

Chris Ward continued this work, showing combined effects of tunnel noise and surface roughness on crossflow-induced transition for this cone [7]. The roughness was varied on the frustum by altering the finish of the temperature-sensitive paint. To make the surface

more rough, the paint had an "orange-peel" finish. The temperature-sensitive paint was only applied to the frustum. Under noisy flow, transition begins on the yaw side of the cone and propagates towards the windward and leeward rays. Surface roughness clearly affects this transition.

It was then decided to alter the roughness of the stainless steel nosetip since the neutral point of the most amplified stationary waves is near the nosetip. The roughness was varied through polishing the steel. The polished nosetip had an average roughness about an order of magnitude less than the machine-finished nosetip. However, there were no large effects when the nosetip roughness was varied [10]. It was thought that the forward-facing step at the nosetip-frustum junction due to the addition of the temperature-sensitive paint was dominating the generation of the stationary crossflow vortices. This forward-facing step was an order of magnitude greater than the average roughness of the machine-finished nosetip [12].

Due in part to budget limitations, Ward's work then shifted towards improving the temperature-sensitive paint technique, with funding from NASA. A method for obtaining quantitative heat transfer from the temperature-sensitive paints has been developed, as described in the next section. Also, a new method of applying the paint was developed, to feather the paint edge so that the magnitude of the forward-facing step is greatly reduced. Both of these developments will be implemented in future experiments. Obtaining global quantitative heat transfer will allow for a better determination of the effect of the varying surface roughness on the stationary crossflow vortices.

15 Obtaining Quantitative Heat Transfer from Temperature-Sensitive Paints

From the beginning, the Purdue Mach-6 quiet nozzle was designed to be the first quiet nozzle with good optical access, although with certain limitations [54]. Since the burst diaphragms must be downstream to permit quiet flow, the windows are pressurized to stagnation conditions, which leads towards the use of plexiglas, which is not brittle, and so less of a safety issue. The windows must be in the nozzle itself, and so should be contoured to match the nozzle shape, which also leads to the use of plexiglas, for affordability. Curved plexiglas windows do not permit the use of schlieren methods, or infrared imaging. Although both of these techniques could be developed by using expensive glass windows, the original design called for the use of Temperature-Sensitive Paint (TSP) to image heat transfer and boundary-layer transition [55]. TSP has been in use for this purpose since ca. 2001, with the help of Prof. Sullivan from Purdue, who worked in this area for many years [56]. The TSP imaging has been very useful, although only for qualitative purposes, since early efforts to infer heat transfer from a series of surface-temperature images were not successful.

After the tunnel became quiet at high Reynolds numbers, in fall 2006, improvements in instrumentation became a higher priority. For complex geometries, it is not always easy to infer the onset of transition from a surface-temperature image. It is much better to measure the surface heat transfer, and infer the onset of transition from where the measurement departs from a laminar computation. The necessary improvements in technique required a multidisciplinary joint effort involving expertise in TSP, heat transfer, and tunnel operations

and needs. Such an effort was funded by a NASA cooperative agreement in Jan. 2008 [57]. Difficulties included the low heat transfer observed on slender models in the tunnel, large heat pulses at startup and shutdown due to the downstream burst-diaphragm valve, and the limited uniformity of the thickness of the insulating and temperature-sensitive paints. As described in Refs. [57, 16] and [15], a promising approach was developed using a sharp 7-deg. cone at zero angle of attack. Aluminum models are painted with a thin insulating layer followed by the TSP. It also turns out to be necessary to install a couple of Schmidt-Boelter gauges, so the TSP can be calibrated using the time-traces from the single-point gauges. These factors in combination have resulted in a simple and practical method that has shown promising results for simple geometries. Although most of this work was funded by NASA, the last part of the Mach-6 tunnel work was also funded by the present AFOSR grant.

16 Effect of Tunnel Noise on Laminar Stagnation-Point Heating

For blunt bodies under some conditions, the measured laminar heating is significantly above the computed value, near the stagnation region [28, 12, 10]. In an attempt to determine if tunnel noise could account for the higher heat transfer, Peter Gilbert carried out measurements on blunt geometries in the Mach-6 quiet tunnel. However, Gilbert found no effect of tunnel noise on the heat transfer. Although this work was primarily funded by NASA, a small part was funded by the present grant. This problem remains of interest and work continues in AEDC Tunnel 9 with support from NASA Johnson. This work also led to a better understanding of the tunnel's ability to start larger models and blunt models [12].

17 Instability and Transition on a Von Karman Ogive

In early summer 2010, Raytheon expressed interest in instability and transition measurements on a Von-Karman ogive-cylinder, for certain DoD applications. Laura Letterman was funded by a Purdue fellowship and needed a topic for her M.S. thesis, so we decided to devote the work to this geometry [29]. Raytheon provided a public-release geometry, some computational results, and some input on the sort of phenomena which were of interest. Letterman tested models with 2-inch and 3-inch base diameters. The larger model did not start at angle of attack. The fairly blunt models tended to be laminar, so most runs were carried out at high unit Reynolds numbers where the tunnel is never quiet. All smooth-body tests under quiet flow were laminar, although there were again some effects of tunnel noise on roughness-induced transition. Although the larger model provided a higher Reynolds number at zero angle of attack, the bow shock reflected back onto the model near the base, making the results more difficult to interpret. The smooth models at zero angle of attack were mostly laminar, with some indications of transition near the aft end of the 3-inch model [15]. The heat transfer is very low on this long model with a blunt nose, so the quality of the TSP images is reduced.

Most of the research was performed using the 2-inch model at 2-deg. angle of attack. The smooth model appeared to transition on the lee side towards the aft end. Although

forward and aft-facing steps had little effect on transition, distributed or isolated roughness did induce transition. There were no indications of second-mode waves, but some indications of first-mode waves.

This work was funded mostly by Letterman's fellowship, with her experimental supplies and tunnel time funded by the present grant. Funds to continue the work are being sought from other DoD sponsors.

18 Summary

The Mach-6 wind tunnel remained quiet through most of the grant period. The quiet-flow Reynolds number fell in late spring 2010 when the nozzle was opened for fit checks of a proposed new throat, but a high-quality repolish yielded record quiet-flow Reynolds numbers in late summer 2010. The nozzle-wall boundary layer remains laminar more than 10 inches beyond the exit for total pressures near 165 psia, and unit Reynolds numbers near 3.7×10^6/ft. It appears that quiet flow can be maintained over the whole length of a slender model for these conditions, for typical model lengths of 1.5 to 3 ft.

Instability and transition measurements were performed for a variety of geometries under a variety of conditions, as reported in 17 conference papers, 8 Master's theses, and two Ph.D. theses. On the HiFire-5 geometry, both the crossflow and second-mode instabilities seem to appear upstream of transition, and tunnel noise affects both. Similar phenomena were observed on the X-51A forebody. Tunnel noise has a significant influence on roughness-induced transition for both configurations, and in general for all configurations studied.

Transition induced by the second-mode instability is probably most critical for slender DoD geometries. The PCB-132 pressure sensors are now in use at many facilities for measuring these waves, thanks in part to support under an AFOSR T&E grant but also the present grant. Second-mode-induced transition is being measured on sharp 7-deg. cones at various wind tunnels to begin to determine the effects of tunnel noise, Mach number, enthalpy and so on. A highly-unstable flared cone was successfully designed, built and tested in order to obtain very large second-mode waves even under quiet flow. Transition to turbulence was recently achieved on such a cone, apparently under fully quiet flow, opening up an experimental path to the study of criteria for the onset of second-mode-induced transition.

Crossflow-induced transition remains critical for slender DoD geometries with three-dimensional flow. A 7-deg. half-angle cone at 6-deg. AOA is being used by several researchers as a simple canonical geometry with which to study this mechanism. Purdue measurements using this geometry continue to show a substantial effect of tunnel noise on the stationary crossflow instability and on transition. It will be necessary to measure both traveling and stationary instabilities plus the secondary instabilities that cause the breakdown of stationary waves. It is also necessary to induce the waves using controlled roughness. Means for doing all these things are still being developed.

Receptivity is to be measured using a laser-induced local perturbation in the freestream, with the results compared to computations by others. The perturber apparatus developed in the Mach-4 quiet tunnel in the 1990's is being adapted to the Mach-6 tunnel. It appears that an acceptable optical apparatus is nearly complete.

Several projects funded primarily by other agencies were completed in good order us-

ing partial funding from the present grant. Temperature-sensitive paint measurements can now be analyzed to determine heat transfer, because of a NASA-funded project that was completed using a small amount of funding from the present grant. Instabilities have been measured in the wake of isolated roughness, opening up an approach to physics-based predictions of transition for such flows; this work was again funded primarily by NASA, but is being completed with funding from the present grant. Second-mode wave packets that grow into young turbulent spots have been generated and measured on the nozzle wall and also on a 7-deg. cone, using support from NDSEG and NSF fellowships, Sandia National Laboratories, and also the present grant. Instability and transition on a Von-Karman ogive-cylinder was measured for Raytheon, using support from a Purdue fellowship and also the present grant. The effect of tunnel noise on stagnation-point laminar heating augmentation was measured using support from NASA, but with some assistance from the present grant.

Measurements in the Mach-6 quiet tunnel are beginning to have an impact for a number of transition problems of interest to the DoD. Pending FY12-16 funding will enable this work to continue towards development of mechanism-based transition estimation methods that can be used to design and develop DoD vehicles.

19 Acknowledgements

Most of the present report is edited from the cited papers, each of which has multiple authors. Portions of the work were also supported by Sandia National Laboratories and by various NASA grants. Since all these grants support related work in the Mach-6 quiet tunnel, they are synergistic in many ways, but an attempt has been made to isolate the AFOSR-supported work in the present report. These complex quiet-tunnel experiments would not have been possible without the support of many organizations and individuals. The measurements reported here were carried out by the following graduate students doing thesis work in the Mach-6 tunnel: Matthew Borg, Thomas Juliano, Katya Casper, Bradley Wheaton, Dennis Berridge, Laura Steen, Amanda Chou, Chris Ward, Peter Gilbert, Laura Letterman and Ryan Luersen. Paul Thomas of American Pride Mold Polishing did an outstanding job of repolishing the nozzle throat in summer 2010.

20 References

[1] Brad M. Wheaton, Thomas J. Juliano, Dennis C. Berridge, Amanda Chou, Peter L. Gilbert, Katya M. Casper, Laura E. Steen, and Steven P. Schneider. Instability and transition measurements in the Mach-6 quiet tunnel. Paper 2009-3559, AIAA, June 2009.

[2] Katya M. Casper, Steven J. Beresh, John F. Henfling, Russell W. Spillers, and Steven P. Schneider. Pressure fluctuations in laminar, transitional, and turbulent hypersonic boundary layers. Paper 2009-4054, AIAA, June 2009. Revised version 6 Nov. 2009.

[3] Christopher R. Alba, Katya M. Casper, Steven J. Beresh, and Steven P. Schneider. Comparison of experimentally measured and computed second-mode disturbances in hypersonic boundary layers. Paper 2010-0897, AIAA, January 2010.

[4] Steven P. Schneider. Summary of hypersonic transition research coordinated through NATO RTO AVT-136. Paper 2010-1466, AIAA, January 2010.

[5] Bradley M. Wheaton and Steven P. Schneider. Roughness-induced instability in a laminar boundary layer at Mach 6. Paper 2010-1574, AIAA, January 2010.

[6] Erick O. Swanson and Steven P. Schneider. Boundary-layer transition on cones at angle of attack in a Mach-6 quiet tunnel. Paper 2010-1062, AIAA, January 2010.

[7] Dennis Berridge, Amanda Chou, Christopher Ward, Laura Steen, Peter Gilbert, Thomas Juliano, Steven Schneider, and Joel Gronvall. Hypersonic boundary-layer transition experiments in a Mach-6 quiet tunnel. Paper 2010-1061, AIAA, January 2010.

[8] Dennis C. Berridge, Katya M. Casper, Shann J. Rufer, Christopher R. Alba, Daniel R. Lewis, Steven J. Beresh, and Steven P. Schneider. Measurements and computations of second-mode instability waves in three hypersonic wind tunnels. Paper 2010-5002, AIAA, June 2010.

[9] Thomas J. Juliano and Steven P. Schneider. Instability and transition on the HIFiRE-5 in a Mach-6 quiet tunnel. Paper 2010-5004, AIAA, June 2010.

[10] Christopher A.C. Ward, Bradley M. Wheaton, Amanda Chou, Peter L. Gilbert, Laura E. Steen, and Steven P. Schneider. Boundary-layer transition measurements in a Mach-6 quiet tunnel. Paper 2010-4721, AIAA, June 2010.

[11] Katya M. Casper, Steven J. Beresh, and Steven P. Schneider. Pressure fluctuations beneath turbulent spots and instability wave packets in a hypersonic boundary layer. Paper 2011-0372, AIAA, January 2011.

[12] Amanda Chou, Bradley M. Wheaton, Christopher A.C. Ward, Peter L. Gilbert, Laura E. Steen, and Steven P. Schneider. Instability and transition research in a Mach-6 quiet tunnel. Paper 2011-0283, AIAA, January 2011.

[13] Katya M. Casper, Steven J. Beresh, and Steven P. Schneider. Spanwise growth of the turbulent spot pressure-fluctuation field in a hypersonic boundary layer. Paper 2011-3873, AIAA, June 2011.

[14] Bradley M. Wheaton, Steven P. Schneider, Matthew D. Bartkowicz, P. K. Subbareddy, and Graham V. Candler. Numerical and experimental comparison of roughness-induced instabilities at Mach 6. Paper 2011-3248, AIAA, June 2011.

[15] Amanda Chou, Christopher A.C. Ward, Laura E. Letterman, Ryan P.K. Luersen, Matthew P. Borg, and Steven P. Schneider. Transition research with temperature-sensitive paints in the Boeing/AFOSR Mach-6 quiet tunnel. Paper 2011-3872, AIAA, June 2011.

[16] Christopher A.C. Ward, Bradley M. Wheaton, Amanda Chou, Dennis C. Berridge, Laura E. Letterman, Ryan P.K. Luersen, and Steven P. Schneider. Hypersonic boundary-layer transition experiments in the Boeing/AFOSR Mach-6 quiet tunnel. Paper 2012-0282, AIAA, January 2012.

[17] Katya M. Casper, Steven J. Beresh, and Steven P. Schneider. Characterization of controlled perturbations in a hypersonic boundary layer. Paper 2012-0281, AIAA, January 2012.

[18] Steven P. Schneider. Hypersonic boundary-layer transition with ablation and blowing. *Journal of Spacecraft and Rockets*, 47(2):225–237, Mar.-Apr. 2010.

[19] Katya M. Casper, Heath B. Johnson, and Steven P. Schneider. Effect of freestream noise on roughness-induced transition for a slender cone. *J. Spacecraft and Rockets*, 48(3):406–413, May-June 2011.

[20] Matthew P. Borg. *Laminar instability and transition on the X-51A*. PhD thesis, School of Aeronautics and Astronautics, Purdue University, August 2009. Available from DTIC as ADA504178.

[21] Thomas J. Juliano. *Instability and Transition on the HiFire-5 in a Mach-6 quiet tunnel*. PhD thesis, School of Aeronautics and Astronautics, Purdue University, August 2010. DTIC citation AD-A528752. Approved for public release.

[22] Katya M. Casper. Hypersonic wind-tunnel measurements of boundary-layer pressure fluctuations. Master's thesis, School of Aeronautics and Astronautics, Purdue University, August 2009.

[23] Bradley M. Wheaton. Roughness-induced instability in a laminar boundary layer at Mach 6. Master's thesis, School of Aeronautics and Astronautics, Purdue University, December 2009.

[24] Dennis C. Berridge. Measurements of second-mode instability waves in hypersonic boundary layers with a high-frequency pressure transducer. Master's thesis, School of Aeronautics and Astronautics, Purdue University, December 2010.

[25] Laura-cheri E. Steen. Characterization and development of nozzles for a hypersonic quiet wind tunnel. Master's thesis, School of Aeronautics and Astronautics, Purdue University, December 2010.

[26] Amanda Chou. Characterization of laser-generated perturbations and instability measurements on a flared cone. Master's thesis, School of Aeronautics and Astronautics, Purdue University, December 2010.

[27] Christopher A.C. Ward. Hypersonic crossflow instability and transition on a circular cone at angle of attack. Master's thesis, School of Aeronautics and Astronautics, Purdue University, December 2010.

[28] Peter L. Gilbert. Effect of tunnel noise on laminar stagnation-point heating at Mach 6. Master's thesis, School of Aeronautics and Astronautics, Purdue University, December 2010.

[29] Laura E. Letterman. Instability and transition on a Von Karman ogive in a Mach-6 quiet tunnel. Master's thesis, School of Aeronautics and Astronautics, Purdue University, December 2011.

[30] I.E. Beckwith and C.G. Miller III. Aerothermodynamics and transition in high-speed wind tunnels at NASA Langley. *Annual Review of Fluid Mechanics*, 22:419–439, 1990.

[31] Steven P. Schneider. Development of hypersonic quiet tunnels. *Journal of Spacecraft and Rockets*, 45(4):641–664, Jul.-Aug. 2008.

[32] Steven P. Schneider, Craig Skoch, Shann Rufer, Shin Matsumura, and Erick Swanson. Transition research in the Boeing/AFOSR Mach-6 quiet tunnel. Paper 2002-0302, AIAA, January 2002.

[33] Steven P. Schneider, Craig Skoch, Shann Rufer, Erick Swanson, and Matt Borg. Bypass transition on the nozzle wall of the Boeing/AFOSR Mach-6 quiet tunnel. Paper 2004-0250, AIAA, January 2004.

[34] Steven P. Schneider. Final report for DURIP grant FA9550-08-1-0437: Towards increased quiet-flow Reynolds number and operability for the 9.5-inch Mach-6 Ludwieg tube. Contractor Report TBD, AFOSR, February 2011.

[35] Matthew P. Borg, Roger Kimmel, and Scott Stanfield. HiFire-5 attachment-line and crossflow instability in a quiet hypersonic wind tunnel. Paper 2011-3247, AIAA, June 2011.

[36] Steven P. Schneider. Final report for AFOSR grant FA9550-08-1-0290 – Hypersonic laminar-turbulent transition on slender cones at zero angle of attack: Measurements in support of mechanism-based models for scaling ground-test data to flight. Final Report AFOSR-TR-11-XXXX, AFOSR, March 2011. Submitted to DTIC. 17 pages.

[37] Malte Estorf, Rolf Radespiel, Steven P. Schneider, Heath B. Johnson, and Stefan Hein. Surface-pressure measurements of second-mode instability in quiet hypersonic flow. Paper 2008-1153, AIAA, January 2008.

[38] Heath Johnson, Christopher Alba, Matthew Bartkowicz, Travis Drayna, and Graham Candler. Design optimization of hypersonic vehicles for boundary layer stability. Paper 2008-6221, AIAA, August 2008.

[39] Mujeeb R. Malik. Hypersonic flight transition data analysis using parabolized stability equations with chemistry effects. *Journal of Spacecraft and Rockets*, 40(3):332–344, May-June 2003.

[40] P. Balakumar and Michael A. Kegerise. Receptivity of hypersonic boundary layers over straight and flared cones. Paper 2010-1065, AIAA, January 2010.

[41] A.C. Laible and H. Fasel. Numerical investigation of hypersonic transition for a flared and a straight cone at Mach 6. Paper 2011-3565, AIAA, June 2011.

[42] F. Li, M. Choudhari, C.-L. Chang, M. Wu, and P.T. Greene. Development and breakdown of Görtler vortices in high-speed boundary layers. Paper 2010-0705, AIAA, June 2010.

[43] J. Sivasubrahmanian and H. Fasel. Numerical investigation of laminar-turbulent transition in a cone boundary layer at Mach 6. Paper 2011-3562, AIAA, June 2011.

[44] Steven P. Schneider. Effects of roughness on hypersonic boundary-layer transition. *Journal of Spacecraft and Rockets*, 45(2):193–209, Mar.-Apr. 2008.

[45] Matthew P. Borg. Characteristics of the contraction of the Boeing/AFOSR Mach-6 quiet tunnel. Master's thesis, School of Aeronautics and Astronautics, Purdue University, December 2005. Available from DTIC as ADA441151.

[46] Steven P. Schneider. Effects of high-speed tunnel noise on laminar-turbulent transition. *Journal of Spacecraft and Rockets*, 38(3):323–333, May–June 2001.

[47] J.D. Schmisseur, Steven H. Collicott, and Steven P. Schneider. Laser-generated localized freestream perturbations in supersonic and hypersonic flows. *AIAA Journal*, 38(4):666–671, April 2000.

[48] J.D. Schmisseur, Steven P. Schneider, and Steven H. Collicott. Supersonic boundary-layer response to optically generated freestream disturbances. *Experiments in Fluids*, 33(2):225–232, August 2002.

[49] Terry R. Salyer, Steven H. Collicott, and Steven P. Schneider. Characterizing laser-generated hot spots for receptivity studies. *AIAA Journal*, 44(12):2871–2878, December 2006.

[50] Dale W. Ladoon, Steven P. Schneider, and John D. Schmisseur. Physics of resonance in a supersonic forward-facing cavity. *J. of Spacecraft and Rockets*, 35(5):626–632, Sept.-Oct. 1998.

[51] Rodrigo Segura. Oscillations in a forward-facing cavity measured using laser-differential interferometry in a hypersonic quiet tunnel. Master's thesis, School of Aeronautics and Astronautics, Purdue University, December 2007. DTIC citation AD-A474770.

[52] Thomas J. Juliano, Rodrigo Segura, Matthew P. Borg, Katya Casper, Michael J. Hannon, Jr, Brad M. Wheaton, and Steven P. Schneider. Starting issues and forward-facing cavity resonance in a hypersonic quiet tunnel. Paper 2008-3735, AIAA, June 2008.

[53] W.A. Engblom, D.B. Goldstein, D. Ladoon, and S.P. Schneider. Fluid dynamics of hypersonic forward-facing cavity flow. Paper 96-0667, AIAA, January 1996.

[54] Steven P. Schneider. Design of a Mach-6 quiet-flow wind-tunnel nozzle using the e**N method for transition estimation. Paper 98-0547, AIAA, January 1998.

[55] T. Liu and J.P. Sullivan. *Pressure and Temperature Sensitive Paints*. Springer, 2005.

[56] Shin Matsumura, Steven P. Schneider, and Scott A. Berry. Flow visualization measurement techniques for high-speed transition research in the Boeing/AFOSR Mach-6 quiet tunnel. Paper 2003-4583, AIAA, July 2003.

[57] John P. Sullivan, Steven P. Schneider, Tianshu Liu, Justin Rubal, Chris Ward, Joseph Dussling, Cody Rice, Ryan Foley, Zeimin Cai, Bo Wang, and Sudesh Woodiga. Quantitative global heat transfer in a Mach-6 quiet tunnel. Technical Report NASA-CR-2012-217331, NASA, February 2012.